PHYSICAL REVIEW D **74,** 014005 (2006)

Shape-function effects and split matching in $B \to X_s \ell^+ \ell^-$

Keith S. M. Lee* and Iain W. Stewart†

Center for Theoretical Physics, Laboratory for Nuclear Science, Massachusetts Institute of Technology, Cambridge, Massachusetts 02139, USA

(Received 10 January 2006; published 7 July 2006)

We derive the triply differential spectrum for the inclusive rare decay $B \to X_s \ell^+ \ell^-$ in the shape-function region, in which X_s is jetlike with $m_X^2 \lesssim m_b \Lambda_{\rm QCD}$. Experimental cuts make this a relevant region. The perturbative and nonperturbative parts of the matrix elements can be defined with the soft-collinear effective theory, which is used to incorporate α_s corrections consistently. We prove that, with a suitable power counting for the dilepton invariant mass, the same universal jet and shape functions appear as in $B \to X_s \gamma$ and $B \to X_u \ell \bar{\nu}$ decays. Parts of the usual $\alpha_s(m_b)$ corrections go into the jet function at a lower scale, and parts go into the nonperturbative shape function. For $B \to X_s \ell^+ \ell^-$, the perturbative series in α_s are of a different character above and below $\mu = m_b$. We introduce a "split matching" method that allows the series in these regions to be treated independently.

DOI: 10.1103/PhysRevD.74.014005 PACS numbers: 13.20.He, 12.38.Bx, 12.39.Hg

I. INTRODUCTION

The B meson is particularly suitable for probing QCD and flavor physics in the standard model, since the large mass of the b quark relative to $\Lambda_{\rm QCD}$ provides a useful expansion parameter, $\Lambda_{\rm QCD}/m_b \sim 0.1$. The study of inclusive B decays circumvents the need for precision hadronic form factors, while still allowing model-independent predictions. Rare inclusive decays, which involve flavor-changing neutral currents (FCNCs), not only allow measurements of CKM matrix elements, in particular V_{ts} and V_{td}, but are also highly sensitive to new physics, since they do not occur at tree level in the standard model.

Among the inclusive rare B decays, the radiative process $B \to X_s \gamma$ has received the most attention, having been measured first by CLEO [1] and subsequently by other experiments [2–5]. These measurements have provided significant constraints on extensions to the standard model. The decay $B \to X_s \ell^+ \ell^-$ is complementary to, and more complicated than, $B \to X_s \gamma$. Its potential for revealing information beyond that supplied by the radiative decay is due to the presence of two extra operators in the effective electroweak Hamiltonian and the availability of additional kinematical variables, such as the dilepton invariant-mass spectrum and the forward-backward asymmetry. Belle and *BABAR* have already made initial measurements of this dilepton process [6–8].

Provided that one makes suitable phase-space cuts to avoid $c\bar{c}$ resonances, $B \to X_s \ell^+ \ell^-$ is dominated by the quark-level process, which was calculated in Ref. [9]. Owing to the disparate scales, $m_b \ll m_W$, one encounters large logarithms of the form $\alpha_s^n(m_b)\log^n(m_b/m_W)$ (leading log[LL]), $\alpha_s^{n+1}(m_b)\log^n(m_b/m_W)$ (next-to-leading log[NLL]), ..., which should be summed. The NLL calculations were completed in Refs. [10,11], and the NNLL analysis, although technically not fully complete, is at a level that the scale uncertainties have been substantially reduced, after the combined efforts of a number of groups [12–16].

Nonperturbative corrections to the quark-level result can also be calculated by means of a local operator product expansion (OPE) [17], with nonperturbative matrix elements defined with the help of the heavy quark effective theory (HQET) [18]. As is the case for $B \to X_s \gamma$ and $B \to X_u \ell \bar{\nu}$, there are no $\mathcal{O}(1/m_b)$ corrections. The $\mathcal{O}(1/m_b^2)$ corrections and OPE were considered in Ref. [19] and subsequently corrected in Ref. [20]. The $\mathcal{O}(1/m_b^3)$ corrections were computed in Ref. [21]. There are also nonperturbative contributions arising from the $c\bar{c}$ intermediate states. The largest $c\bar{c}$ resonances, i.e. the J/ψ and ψ', can be removed by suitable cuts in the dilepton mass spectrum. It is generally believed that the operator product expansion holds for the computation of the dilepton invariant mass as long as one avoids the region with the first two narrow resonances, although no complete proof of this (for the full operator basis) has been given. A picture for the structure of resonances can be obtained using the model of Krüger and Sehgal [22], which estimates factorizable contributions based on a dispersion relation and experimental data on $\sigma(e^+e^- \to c\bar{c} + \text{hadrons})$. Nonfactorizable effects have been estimated in a model-independent way by means of an expansion in $1/m_c$ [23], which is valid only away from the resonances.

Staying away from the resonance regions in the dilepton mass spectrum leaves two perturbative windows, the low- and high-q^2 regions, corresponding to $q^2 \leq 6$ GeV^2 and $q^2 \geq 14.4$ GeV^2 respectively. These have complementary advantages and disadvantages [16]. For example, the latter has significant $1/m_b$ corrections but negligible scale and charm-mass dependence, whereas the former has small $1/m_b$ corrections but non-negligible scale and charm-

*Electronic address: ksml@mit.edu
†Electronic address: iains@mit.edu

mass dependence. The low-q^2 region has a high rate compared to the high-q^2 region and so experimental spectra will become precise for this region first. However, at low q^2 an additional cut is required, making measurements less inclusive. In particular, a hadronic invariant-mass cut is imposed in order to eliminate the combinatorial background, which includes the semileptonic decay $b \to c(\to se^+\nu)e^-\bar{\nu} = b \to se^+e^-$ + missing energy. The latest analyses from *BABAR* and Belle impose cuts of $m_X \leq 1.8$ GeV and $m_X \leq 2.0$ GeV respectively [6–8], which in the B-meson rest frame correspond to $q^0 \gtrsim 2.3$ GeV and put the decay rate in the so-called shape-function region [24]. This cut dependence has so far been analyzed only in the Fermi-motion model [25].

Existing calculations for $B \to X_s\ell^+\ell^-$ are based on a local operator product expansion in Λ_{QCD}/m_b. When $m_X^2 \lesssim m_b\Lambda \sim (2\ \text{GeV})^2$, this operator product expansion breaks down, and, instead of depending on nonperturbative parameters $(\lambda_1, \lambda_2, \ldots)$ that are matrix elements of local operators, the decay rates depend on nonperturbative functions. Furthermore, in this region the standard perturbative α_s corrections to the partonic process $b \to s\ell^+\ell^-$ do not apply, since some of these corrections become nonperturbative. Thus, even at leading order there does not exist in the literature a model-independent computation of the $B \to X_s\ell^+\ell^-$ decay rate that can be compared directly with the data at low q^2.

Here we study $B \to X_s\ell^+\ell^-$ $(\ell = e, \mu)$ in the shape-function region for the first time. The relevant scales are $m_W^2 \gg m_b^2 \gg m_b\Lambda_{QCD} \gg \Lambda_{QCD}^2$. In this paper we derive the proper theoretical expression for the leading-order triply differential decay rate, which incorporates nonperturbative effects that appear at this order and a correct treatment of the perturbative corrections at each of the scales. Using the soft-collinear effective theory (SCET) [26–29] we prove that the nonperturbative dynamics governing the measurable low-q^2 spectra in $B \to X_s\ell^+\ell^-$ is determined by the same universal shape function as in endpoint $B \to X_u\ell\bar{\nu}$ and $B \to X_s\gamma$ decays. We also prove that the decay rate can be split into a product of scale-invariant terms, capturing physics at scales above and below m_b. We show that this procedure, which we call "split matching", can be used to deal with a tension between the perturbative corrections that come from these two regions. Implications for relating the $B \to X_s\ell^+\ell^-$ measurements with the m_X cut to the Wilson coefficients are presented in a companion publication [30].

In the shape-function region, the set of outgoing hadronic states becomes jetlike and the relevant degrees of freedom are collinear and ultrasoft modes. This is why the appropriate theoretical method is SCET. The endpoint region has been the focus of much work in the context of $B \to X_s\gamma$ and $B \to X_u\ell\bar{\nu}$ (see e.g. Refs. [24,29,31–43]). In $B \to X_u\ell\bar{\nu}$ this is because of the cuts used to eliminate the dominant $b \to c$ background. In $B \to X_s\gamma$, it is known that

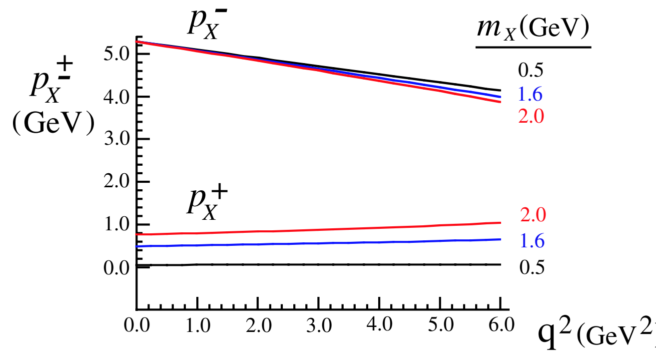

FIG. 1 (color online). The kinematic range for p_X^- and p_X^+ given the experimental cuts of $q^2 < 6$ GeV^2 and $m_X \leq 2.0$ GeV for $B \to X_s\ell^+\ell^-$.

cuts with $q^0 \gtrsim 2.1$ GeV put us in the shape-function region.[1]

In the small-q^2 region of $B \to X_s\ell^+\ell^-$ with $q^0 \gtrsim 2.3$ GeV, shape-function effects also dominate rather than the expansion in local operators. To see this, we note that the m_X cut causes $2m_BE_X = m_B^2 + m_X^2 - q^2 \gg m_X^2$. Decomposing $2E_X = p_X^+ + p_X^-$ with $m_X^2 = p_X^-p_X^+$, we see that the X_s is jetlike with $p_X^- \gg p_X^+$, and the restricted sum over states in the X_s causes the nonperturbative shape functions to become important. For the experimental cuts on q^2 and m_X, values for $p_X^\pm$ are shown in Fig. 1. It should be clear from this figure that the measurable spectrum is dominated by decays for which $p_X^- \gg p_X^+$.

To compute $B \to X_s\ell^+\ell^-$ in the shape-function region with renormalization-group evolution requires the following steps:

(i) matching the standard model at $\mu \simeq m_W$ on to H_W,
(ii) running H_W to $\mu \simeq m_b$,
(iii) matching at $\mu \simeq m_b$ on to operators in SCET,
(iv) running in SCET to $\mu \simeq \sqrt{m_b\Lambda}$,
(v) computation of the imaginary part of forward-scattering time-ordered products in SCET at $\mu \simeq \sqrt{m_b\Lambda}$. This leads to a separation of scales in a factorization theorem, which at LO takes the form[2]

$$d^3\Gamma^{(0)} = H\int dk\mathcal{J}^{(0)}(k)f^{(0)}(k),$$

with perturbative H and $\mathcal{J}^{(0)}$, and the LO nonperturbative shape function $f^{(0)}$,
(vi) evolution of the shape function $f^{(0)}$ from Λ_{QCD} up to $\mu \simeq \sqrt{m_b\Lambda_{QCD}}$.

[1] In Ref. [44] it was pointed out that even a cut of $E_\gamma \geq E_0 = 1.8$ GeV, corresponding to $m_X \lesssim 3$ GeV, might not guarantee that a theoretical description in terms of the local OPE is sufficient, owing to sensitivity to the scale $\Delta = m_b - 2E_0$ in power and perturbative corrections. Using a multiscale OPE with an expansion in Λ/Δ allows the shape-function and local OPE regions to be connected [33,34,44].

[2] Note that the operator product expansion used here occurs at $\mu \simeq \sqrt{m_b\Lambda}$, rather than at m_b^2, as in the standard local OPE.

For the shape-function decay rate, steps (i–ii) are the same as the local OPE results for $B \to X_s \ell^+ \ell^-$. Furthermore, based on the structure of leading-order SCET operators that we find for $B \to X_s \ell^+ \ell^-$, we demonstrate that results for other inclusive endpoint analyses can be used in steps (iv) and (vi) [26,27,34].[3] Because of this our computations focussed on steps (iii) and (v). In step (iii) we show how to implement the split-matching procedure to formulate the perturbative corrections, which we elaborate on below. In step (v) we derive a factorization theorem for $B \to X_s \ell^+ \ell^-$. This includes computing the hard coefficient functions H at NLL order and formulating the structure of these terms to all orders in α_s. It also includes a derivation of formulas for the decay rate and forward-backward asymmetry that properly take into account the effect of the current experimental cuts and the perturbative and nonperturbative corrections.

At leading order in the power expansion the result of steps (i)-(vi) takes the schematic form

$$d^3\Gamma^{(0)} = \mathcal{E}(\mu_W) U_W(\mu_W, \mu_0) \mathcal{B}(\mu_0) U_H(\mu_0, \mu_i) \mathcal{J}(\mu_i) U_S(\mu_i, \mu_\Lambda) f^{(0)}(\mu_\Lambda),$$
$$\mu_W \simeq m_W, \qquad \mu_0 \simeq m_b, \qquad \mu_i \simeq (m_b \Lambda)^{1/2}, \qquad \mu_\Lambda \simeq 1 \text{ GeV}, \tag{1}$$

where $\mathcal{E}$, $\mathcal{B}$ and $\mathcal{J}$ represent matching at various scales, and U_W, U_H and U_S represent the running between these scales. Equation (1) shows only the scale dependence explicitly, not the kinematic dependences or the convolutions between $\mathcal{J}$, U_S, and $f^{(0)}$, which we describe later on.

In a standard application of renormalization-group improved perturbation theory (LL, NLL, NNLL, etc.), the results at each stage of matching and running are tied together, as depicted in Eq. (1). Usually this would not be a problem, but for $B \to X_s \ell^+ \ell^-$ the nature of the perturbative expansion above and below $\mu \simeq m_b$ is different. Above $\mu \simeq m_b$ the series of $(\alpha_s \ln)^k$ terms are of the traditional form, with a basis of ~ 10 operators (including four-quark operators), whose mixing is crucial. Below $\mu \simeq m_b$ we demonstrate that the evolution is universal (to all orders in α_s) for the leading-order operators, but there are Sudakov double logarithms of the ratios of scales, which give a more complicated series. It turns out to be convenient to decouple these two stages of resummation so that one can consider working to different orders in the α_s expansion above and below $\mu = m_b$. There is a simple reason why this decoupling is important: for $\mu \geq m_b$ the power counting and running are for currents in the electroweak Hamiltonian and dictate treating $C_9 \sim 1/\alpha_s$ with $C_7 \sim 1$ and $C_{10} \sim 1$. However, at $\mu = m_b$ the coefficients C_9 and C_{10} are numerically comparable. For $\mu \leq m_b$ in the shape-function region we must organize the power counting and running for time-ordered products of currents in SCET rather than amplitudes, and it would be vexing to have to include terms $\propto C_9^2$ to $\mathcal{O}(\alpha_s^2)$ before including the C_{10}^2 and C_7^2 terms at order $\mathcal{O}(\alpha_s^0)$. Thus, once we are below the scale m_b, a counting with $C_9 \sim C_{10} \sim C_7 \sim 1$ is more appropriate.

To decouple these two regions for $B \to X_s \ell^+ \ell^-$ decays we make use of two facts: (i) for $\mu \geq m_b$ the operator $\mathcal{O}_{10}$ involves a conserved current and has no operators mixing into it, so it does not have an anomalous dimension, and (ii) for $\mu \leq m_b$ all LO biquark operators in the soft-collinear effective theory have the same anomalous dimension [27]. We shall show that the operators for $B \to X_s \ell^+ \ell^-$ are related to these biquark operators. These properties ensure that we can separate the perturbative treatments in these two regions at any order in perturbation theory. This is done by introducing two matching scales, $\mu_0 \simeq m_b$ and $\mu_b \simeq m_b$. The two aforementioned facts allow us to write

$$\begin{aligned} &U_W(\mu_W, \mu_0) \mathcal{B}(\mu_0) U_H(\mu_0, \mu_i) \\ &\quad = U_W(\mu_W, \mu_0) \mathcal{B}(\mu_0, \mu_b) U_H(\mu_b, \mu_i) \\ &\quad = U_W(\mu_W, \mu_0) B_1(\mu_0) B_2(\mu_b) U_H(\mu_b, \mu_i), \end{aligned} \tag{2}$$

with well-defined B_1 and B_2. We define $B_2(\mu_b)$ by using the matching for the operator $\mathcal{O}_{10}$ and extend this to find B_2 matching coefficients for the other operators using property (ii) above. The remaining contributions match on to B_1. Diagrams which are related to the anomalous dimension for $\mu \geq m_b$ end up being matched at the scale μ_0 on to B_1, while those related to anomalous dimensions for $\mu \leq m_b$ are matched at a different scale, μ_b, on to B_2. This leaves

$$\begin{aligned} d^3\Gamma^{(0)} = &[\mathcal{E}(\mu_W) U_W(\mu_W, \mu_0) B_1(\mu_0)][B_2(\mu_b) U_H(\mu_b, \mu_i) \\ &\times \mathcal{J}(\mu_i) U_S(\mu_i, \mu_\Lambda) f^{(0)}(\mu_\Lambda)], \end{aligned} \tag{3}$$

which is the product of two pieces that are separately μ-independent. We refer to this procedure as "split matching" because formally we match diagrams at two scales rather than at a single scale. The two matching μ's are

[3] In step (iv) we can run the hard functions down using results from Refs. [26,27]. In step (vi) we can run the shape function up to the intermediate scale using the simple result from Ref. [34]. An equally valid option would be to evolve the perturbative parts of the rate down to a scale $\mu \simeq 1$ GeV, as considered earlier [26,33,42,45].

"split" because they are parametrically similar in the power-counting sense.

We organize the remainder of our paper as follows. We begin by using split matching to determine the hard matching functions, $\mathcal{B} = B_1 B_2$, for $B \to X_s \ell^+ \ell^-$ in SCET; this is one of the main points of our paper. It is discussed in Sec. II A at leading power and one-loop order (including both bottom-, charm-, and light-quark loops and other virtual corrections). The extension to higher orders is also illustrated. Steps (i) and (ii) are summarized in Sec. II A, together with Appendix A. In Sec. II B we discuss the running for step (iv) and give a brief derivation of why the anomalous dimension is independent of the Dirac structure to all orders in α_s. In Sec. II C, we discuss the basic ingredients for the triply differential decay rate and the forward-backward asymmetry in terms of hadronic tensors. A second main point of our paper is the SCET matrix-element computation for $B \to X_s \ell^+ \ell^-$, step (v), which is performed in Sec. II D. In Sec. II E we review the running for the shape function, step (vi). In Sec. III we present our final results for the differential decay rates at leading order in the power expansion, including all the ingredients from Sec. II and incorporating the relevant experimental cuts. The triply differential spectrum and doubly differential spectra are derived in subsections III A, III B, III C, and III D. Readers interested only in our final results may skip directly to Sec. III. We compare numerical results for matching coefficients at m_b with terms in the local OPE in Sec. III E. In Appendix B we briefly comment on how our analysis will change if we assume a parametrically small dilepton invariant mass, $q^2 \sim \lambda^2$, rather than the scaling $q^2 \sim \lambda^0$ used in the body of the paper. (For the case $q^2 \sim \lambda^2$, the rate for $B \to X_s \ell^+ \ell^-$ would *not* be determined by a factorization theorem with the same structure as for $B \to X_u \ell \bar{\nu}$.)

II. ANALYSIS IN THE SHAPE-FUNCTION REGION

A. Matching on to SCET

We begin by reviewing the form of the electroweak Hamiltonian obtained after evolution down to the scale $\mu \simeq m_b$, and then perform the leading-order matching of this Hamiltonian on to operators in SCET. For the treatment of γ_5 we use the NDR scheme throughout. Below the scale $\mu = m_W$, the effective Hamiltonian for $b \to s\ell^+\ell^-$ takes the form [9]

$$\mathcal{H}_W = -\frac{4G_F}{\sqrt{2}} V_{tb} V_{ts}^* \sum_{i=1}^{10} C_i(\mu) \mathcal{O}_i(\mu), \tag{4}$$

where we have used unitarity of the CKM matrix to remove $V_{cb}V_{cs}^*$ dependence and have neglected the tiny $V_{ub}V_{us}^*$ terms. The operators $\mathcal{O}_i(\mu)$ are

$$\begin{aligned}
\mathcal{O}_1 &= (\bar{s}_{L\alpha}\gamma_\mu b_{L\beta})(\bar{c}_{L\beta}\gamma^\mu c_{L\alpha}),\\
\mathcal{O}_2 &= (\bar{s}_{L\alpha}\gamma_\mu b_{L\alpha})(\bar{c}_{L\beta}\gamma^\mu c_{L\beta}),\\
\mathcal{O}_3 &= (\bar{s}_{L\alpha}\gamma_\mu b_{L\alpha}) \sum_{q=u,d,s,c,b} (\bar{q}_{L\beta}\gamma^\mu q_{L\beta}),\\
\mathcal{O}_4 &= (\bar{s}_{L\alpha}\gamma_\mu b_{L\beta}) \sum_{q=u,d,s,c,b} (\bar{q}_{L\beta}\gamma^\mu q_{L\alpha}),\\
\mathcal{O}_5 &= (\bar{s}_{L\alpha}\gamma_\mu b_{L\alpha}) \sum_{q=u,d,s,c,b} (\bar{q}_{R\beta}\gamma^\mu q_{R\beta}),\\
\mathcal{O}_6 &= (\bar{s}_{L\alpha}\gamma_\mu b_{L\beta}) \sum_{q=u,d,s,c,b} (\bar{q}_{R\beta}\gamma^\mu q_{R\alpha}),\\
\mathcal{O}_7 &= \frac{e}{16\pi^2}\bar{s}\sigma_{\mu\nu}F^{\mu\nu}(\bar{m}_b P_R + \bar{m}_s P_L)b,\\
\mathcal{O}_8 &= \frac{g}{16\pi^2}\bar{s}_\alpha T^a_{\alpha\beta}\sigma_{\mu\nu}(\bar{m}_b P_R + \bar{m}_s P_L)b_\beta G^{a\mu\nu},\\
\mathcal{O}_9 &= \frac{e^2}{16\pi^2}\bar{s}_{L\alpha}\gamma^\mu b_{L\alpha}\bar{\ell}\gamma_\mu\ell,\\
\mathcal{O}_{10} &= \frac{e^2}{16\pi^2}\bar{s}_{L\alpha}\gamma^\mu b_{L\alpha}\bar{\ell}\gamma_\mu\gamma_5\ell,
\end{aligned} \tag{5}$$

where $P_{R,L} = (1 \pm \gamma_5)/2$. In the following, we shall neglect the mass of the strange quark in $\mathcal{O}_{7,8}$. For our analysis, m_s is not needed as a regulator for IR divergences, which are explicitly cut off by nonperturbative scales $\sim\Lambda_{\rm QCD}$. In the shape-function region, the m_s dependence is small and was computed in Ref. [46]. Nonperturbative sensitivity to m_s shows up only at subleading power, while computable $\mathcal{O}(m_s^2/m_b\Lambda_{\rm QCD})$ jet-function corrections are numerically smaller than the $\Lambda_{\rm QCD}/m_b$ power corrections.

At NLL order, one requires the NLL Wilson coefficient of $\mathcal{O}_9$ and the LL coefficients of the other operators. For $\mathcal{O}_{7,9,10}$ these are given by [10,11]

$$\begin{aligned}
C_7^{\rm NDR}(\mu) &= r_0^{-16/23}C_7(M_W) + \frac{8}{3}(r_0^{-14/23} - r_0^{-16/23})C_8(M_W)\\
&\quad + \sum_{i=1}^{8} t_i r_0^{-a_i},\\
C_9^{\rm NDR}(\mu) &= P_0^{\rm NDR}(\mu) + \frac{Y(m_t^2/M_W^2)}{\sin^2\theta_W} - 4Z(m_t^2/M_W^2)\\
&\quad + P_E(\mu)E(m_t^2/M_W^2),\\
C_{10}(\mu) &= C_{10}(M_W) = -\frac{Y(m_t^2/M_W^2)}{\sin^2\theta_W},
\end{aligned} \tag{6}$$

where $C_7(m_W)$, $C_8(m_W)$ and the Inami-Lim functions Y, Z, and E are obtained from matching at $\mu = m_W$, and are given in Appendix A. The μ-dependent factors include [10,11]

$$P_0^{\rm NDR}(\mu) = \frac{\pi}{\alpha_s(M_W)}\Big(-0.1875 + \sum_{i=1}^{8} p_i r_0^{-a_i-1}\Big) + 1.2468 + \sum_{i=1}^{8} r_0^{-a_i}(\rho_i^{\rm NDR} + s_i r_0^{-1}),$$
$$P_E(\mu) = 0.1405 + \sum_{i=1}^{8} q_i r_0^{-a_i-1}, \qquad r_0 = \frac{\alpha_s(\mu)}{\alpha_s(m_W)}. \quad (7)$$

The numbers t_i, a_i, $\rho_i^{\rm NDR}$, s_i, q_i that appear here are listed in Appendix A. Results for the running coefficients of the four-quark operators, $C_{1-6}(\mu)$, can be found in Ref. [10]. We have modified the standard notation slightly (e.g. $r_0(\mu)$) to conform with additional stages of the RG evolution discussed in Secs. II B and II E. Contributions beyond NLL will be mentioned below.

At a scale $\mu \approx m_b$, we need to match $b \to s\ell^+\ell^-$ matrix elements of $\mathcal{H}_W$ on to matrix elements of operators in SCET with a power expansion in the small parameter λ, where $\lambda^2 = \Lambda_{\rm QCD}/m_b$. For convenience, we refer to the resulting four-fermion scalar operators in SCET as "currents" and use the notation $J_{\ell\ell}$. In SCET we also need the effective Lagrangians. The heavy quark in the initial state is matched on to an HQET field h_v, and the light energetic strange quark is matched on to a collinear field ξ_n. For the leading-order analysis in Λ/m_b we need only the lowest-order terms,

$$\mathcal{H}_W = -\frac{G_F\alpha}{\sqrt{2}\pi}(V_{tb}V_{ts}^*)J_{\ell\ell}^{(0)}, \qquad \mathcal{L} = \mathcal{L}_{\rm HQET}^{(0)} + \mathcal{L}_{\rm SCET}^{(0)}, \quad (8)$$

where $J_{\ell\ell}^{(0)}$ is the LO operator and the quark contributions to the HQET and SCET actions are

$$\mathcal{L}_{\rm HQET}^{(0)} = \bar{h}_v iv\cdot D_{us} h_v,$$
$$\mathcal{L}_{\rm SCET}^{(0)} = \bar{\xi}_n\Big[in\cdot D_c + i\not{D}_c^{\perp}\frac{1}{i\bar{n}\cdot D_c}i\not{D}_c^{\perp}\Big]\frac{\bar{\not{n}}}{2}\xi_n. \quad (9)$$

The covariant derivatives D_{us} and D_c involve ultrasoft and collinear gluons, respectively, and we have made a field redefinition on the collinear fields to decouple the ultrasoft gluons at LO [29]. For convenience, we define the objects

$$\mathcal{H}_v = Y^\dagger h_v, \qquad \psi_{us} = Y^\dagger q_{us}, \qquad \mathcal{D}_{us} = Y^\dagger D_{us} Y$$
$$\chi_n = W^\dagger \xi_n, \qquad \mathcal{D}_c = W^\dagger D_c W,$$
$$ig\mathcal{B}_c^\mu = \Big[\frac{1}{\bar{\mathcal{P}}}W^\dagger[i\bar{n}\cdot D_c, iD_c^\mu]W\Big], \quad (10)$$

which contain ultrasoft and collinear Wilson lines,

$$Y(x) = P\exp\Big(ig\int_{-\infty}^0 ds\, n\cdot A_{us}(x+ns)\Big) \quad (11)$$

and

$$W(x) = P\exp\Big(ig\int_{-\infty}^0 ds\bar{n}\cdot A_n(x+s\bar{n})\Big), \quad (12)$$

as well as the label operator $\bar{\mathcal{P}}$ [28].

To simplify the analysis we treat both m_c and m_b as hard scales and integrate out both charm and bottom loops at $\mu \simeq m_b$. At leading order in SCET, the currents that we match on to are

$$J_{\ell\ell}^{(0)} = \sum_{i=a,b,c} C_{9i}(s)(\bar{\chi}_{n,p}\Gamma_i^{(v)\mu}\mathcal{H}_v)(\bar{\ell}\gamma_\mu\ell) + \sum_{i=a,b,c} C_{10i}(s)(\bar{\chi}_{n,p}\Gamma_i^{(v)\mu}\mathcal{H}_v)(\bar{\ell}\gamma_\mu\gamma_5\ell) - \sum_{j=a,\dots,d} C_{7j}(s)2m_B(\bar{\chi}_{n,p}\Gamma_j^{(t)\mu}\mathcal{H}_v)(\bar{\ell}\gamma_\mu\ell), \quad (13)$$

where the sum is over Dirac structures to be discussed below. The simple structure of these LO SCET operators is quite important to our analysis: for example, by power counting there are no four-quark operators that need to be included in SCET at this order. In Eq. (13) two auxiliary four-vectors appear, v^μ and n^μ. The B momentum, total momentum of the leptons, and jet momentum (sum of the four-momenta of all the hadrons in X_s) are

$$p_B^\mu = m_B v^\mu, \qquad q^\mu = p_{\ell^+}^\mu + p_{\ell^-}^\mu,$$
$$p_X^\mu = n\cdot p_X\frac{\bar{n}^\mu}{2} + \bar{n}\cdot p_X\frac{n^\mu}{2}, \quad (14)$$

respectively. Here $v^2 = 1$ and n^μ and $\bar{n}^\mu$ are lightlike vectors, which satisfy $n^2 = \bar{n}^2 = 0$ and $n\cdot\bar{n} = 2$. The components of a vector can then be written as $(p^+, p^-, p_\perp) = (n\cdot p, \bar{n}\cdot p, p_\perp^\mu)$. We use a frame in which $q_\perp^\mu = v_\perp^\mu = 0$ and $v^\mu = (n^\mu + \bar{n}^\mu)/2$. Since $p_X = m_B v - q$ we have

$$p_X^2 = m_X^2 = \bar{n}\cdot p_X n\cdot p_X$$
$$= m_B^2 + q^2 - m_B(n\cdot q + \bar{n}\cdot q),$$
$$q^2 = \bar{n}\cdot q n\cdot q,$$
$$\bar{n}\cdot p_X = m_B - \bar{n}\cdot q,$$
$$n\cdot p_X = m_B - n\cdot q. \quad (15)$$

For later convenience we define the hadronic dimensionless variables

$$x_H = \frac{2E_{\ell^-}}{m_B}, \qquad \bar{y}_H = \frac{\bar{n}\cdot p_X}{m_B},$$
$$u_H = \frac{n\cdot p_X}{m_B}, \qquad y_H = \frac{q^2}{m_B^2}. \quad (16)$$

In SCET the total partonic $\bar{n}\cdot p$ momentum of the jet is a hard momentum $\sim m_b$ and also appears in the SCET Wilson coefficients. At LO, $\bar{n}\cdot p = (m_b^2 - q^2)/m_b$ and demanding that $\bar{n}\cdot p$ is large means only that q^2 cannot be too close to m_b^2. For example, neither $q^2 \approx 0$ nor

$q^2 \approx m_b^2/2$ modifies the power counting for $\bar{n}\cdot p$. Thus, there is no requirement to impose a scaling that q^2 be small. For convenience, in the hard coefficients we write

$$C(\bar{n}\cdot p, m_b, \mu_0, \mu_b) \to C(s, m_b, \mu_0, \mu_b), \qquad s = \frac{q^2}{m_b^2}, \tag{17}$$

since the partonic variable s is a more natural choice in $b \to s\ell^+\ell^-$ and is equivalent at LO. For purposes of power counting in this paper we count $s \sim \lambda^0$. We shall see in Sec. III E that varying s causes a very mild change in the coefficients. In Appendix B we briefly explore a different scenario, in which $s \sim \lambda^2$. A distinction between two matching scales μ_0 and μ_b is made in C in order to separate the decay rate into two μ-independent pieces, as displayed in Eq. (3). For power-counting purposes, $\mu_0 \sim \mu_b \sim m_b$ and formally $\mu_0 \geq \mu_b$. For numerical work one can take $\mu_0 = \mu_b$.

In Eq. (13) we begin with a complete set of Dirac structures for the vector and tensor currents in SCET, namely

$$\begin{aligned} \Gamma^{(v)}_{a-c} &= P_R\left\{\gamma^\mu, v^\mu, \frac{n^\mu}{n\cdot v}\right\}, \\ \Gamma^{(t)}_{a-d} &= P_R\frac{q_\tau}{q^2}\left\{i\sigma^{\mu\tau}, \gamma^{[\mu}v^{\tau]}, \frac{\gamma^{[\mu}n^{\tau]}}{n\cdot v}, \frac{n^{[\mu}v^{\tau]}}{n\cdot v}\right\}. \end{aligned} \tag{18}$$

These come with Wilson coefficients $C_{9a,b,c}$ and $C_{7a,b,c,d}$ respectively. This basis is over-complete for $B \to X_s\ell^+\ell^-$, but considering a redundant basis makes it easy to incorporate pre-existing perturbative calculations for the currents into our computations. Only the coefficients $C_{7a,9a}$ appear at tree level, but for heavy-to-light currents it is known that the other structures become relevant once perturbative corrections are included. For simplicity of notation, we treat the $1/q^2$ photon propagator in $\Gamma^{(t)}_j$ as part of the effective-theory operator.[4]

To further reduce the basis in Eq. (18) we can use (i) current conservation, $q^\mu\bar{\ell}\gamma_\mu\ell = 0$, (ii) $q^\mu\bar{\ell}\gamma_\mu\gamma_5\ell = 0$ for massless leptons, (iii) a reduction of the tensor $\Gamma^{(t)}$ Dirac structures into vector structures, since they are all contracted with q_τ. Constraint (ii) allows us to eliminate C_{10c}. Taken together, constraints (i) and (iii) allow us to reduce the seven terms C_{9i} and C_{7i} to two independent coefficients. For our new basis of operators we take

$$\begin{aligned} J^{(0)}_{\ell\ell} &= \mathcal{C}_9(\bar{\chi}_{n,p}P_R\gamma^\mu\mathcal{H}_v)(\bar{\ell}\gamma_\mu\ell) \\ &\quad - \mathcal{C}_7\frac{2m_Bq_\tau}{q^2}(\bar{\chi}_{n,p}P_Ri\sigma^{\mu\tau}\mathcal{H}_v)(\bar{\ell}\gamma_\mu\ell) \\ &\quad + \mathcal{C}_{10a}(\bar{\chi}_{n,p}P_R\gamma^\mu\mathcal{H}_v)(\bar{\ell}\gamma_\mu\gamma_5\ell) \\ &\quad + \mathcal{C}_{10b}(\bar{\chi}_{n,p}P_Rv^\mu\mathcal{H}_v)(\bar{\ell}\gamma_\mu\gamma_5\ell), \end{aligned} \tag{19}$$

and find that

$$\begin{aligned} \mathcal{C}_9 &= C_{9a} + \frac{C_{9b}}{2} - \frac{m_B}{n\cdot q}C_{7b} \\ &\quad + \frac{2m_B(C_{7c}-C_{7d}) + n\cdot qC_{9c}}{n\cdot q - \bar{n}\cdot q}, \\ \mathcal{C}_7 &= C_{7a} - \frac{C_{7b}}{2} - \frac{\bar{n}\cdot q}{4m_B}C_{9b} + \frac{1}{n\cdot q - \bar{n}\cdot q} \\ &\quad \times\left[\frac{-q^2}{2m_B}C_{9c} - n\cdot qC_{7c} + \bar{n}\cdot qC_{7d}\right], \\ \mathcal{C}_{10a} &= C_{10a}, \\ \mathcal{C}_{10b} &= C_{10b} + \frac{2n\cdot q}{n\cdot q - \bar{n}\cdot q}C_{10c}. \end{aligned} \tag{20}$$

Our Dirac structures for the $\mathcal{C}_9$ and $\mathcal{C}_7$ terms in Eq. (19) were deliberately chosen, in order to make results for the decay rates appear as much as possible like those in the local OPE. The fact that the basis of SCET operators for $B \to X_s\ell^+\ell^-$ involves only bilinear hadronic currents at LO means that in the leading-order factorization theorem we find the exact same nonperturbative shape function as for $B \to X_s\gamma$ and $B \to X_u\ell\bar{\nu}$. This is immediately evident from the operator-based proof of factorization in Ref. [29], for example. While the coefficients C_{9i}, C_{7i}, C_{10i} in Eq. (13) are functions only of $s = (n\cdot q)(\bar{n}\cdot q)/m_b^2$, the reduction of the basis of operators brings in additional kinematic dependence on $\bar{n}\cdot q$ and $n\cdot q$ for the $\mathcal{C}_i$'s (which is also the case in analyzing exclusive dilepton decays [47]). At tree level we have $\mathcal{O}_{9,10}$ contributing to C_{9a} and C_{10a}, and a contribution from $\mathcal{O}_7$ with the photon producing an $\ell^+\ell^-$ pair, which give

$$\begin{aligned} \mathcal{C}_9 &= C_9^{\rm NDR}(\mu_0), \qquad \mathcal{C}_7 = \frac{\bar{m}_b(\mu_0)}{m_B}C_7^{\rm NDR}(\mu_0), \\ \mathcal{C}_{10a} &= C_{10}, \qquad \mathcal{C}_{10b} = 0. \end{aligned} \tag{21}$$

Beyond tree level there will be C_7 dependence in $\mathcal{C}_9$, and C_9 dependence in $\mathcal{C}_7$. Equation (21) indicates that with our choice of basis the same short-distance dependence dominates in SCET: $\mathcal{C}_9 \approx C_9$, etc. We explore this further in Sec. III E. In Eq. (21) there is no distinction as to whether this matching is done at $\mu = \mu_0$ or $\mu = \mu_b$. The effective-theory operator in Eq. (19) was defined with a factor of m_B pulled out so that the μ-dependent factors $\bar{m}_bC_7^{\rm NDR}$ are contained in the coefficients $\mathcal{C}_7$.

At one-loop order, the full-theory diagrams needed for the matching are shown in Fig. 2 (plus wave-function

[4]If we instead demand that the momentum q^2 be collinear in the $\bar{n}$ direction, with $s \sim \lambda^2$, then the SCET operator with a photon field strength should be kept, and will then be contracted with an operator with collinear leptons within SCET. In this case there will also be additional four-quark operators needed in the basis in Eq. (19).

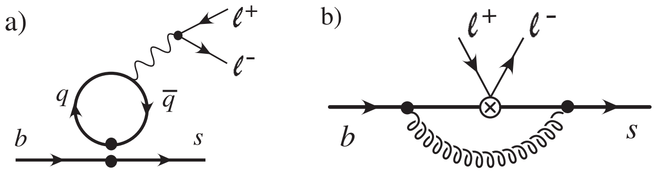

FIG. 2. Graphs from H_W for matching on to SCET.

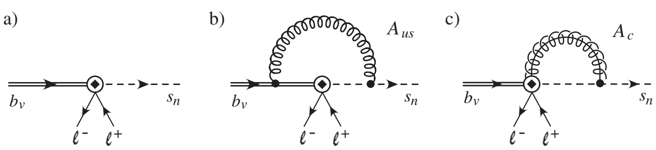

FIG. 3. Graphs in SCET for the matching computation.

renormalization, which is not shown). At this order the four-quark operators $\mathcal{O}_{1-6}$ contribute through Fig. 2(a). The one-loop graphs in SCET with the operators in Eq. (19) are shown in Fig. 3 (plus wave-function renormalization, which is not shown). There are no graphs with four-quark operators within SCET since we treat $q^2 \sim \lambda^0$, so Fig. 2(a) matches directly on to $\mathcal{C}_9$.

As discussed in the introduction, we perform a split-matching procedure from the full theory above m_b on to SCET below m_b, making use of two matching scales μ_0 and μ_b. Contributions from this stage of matching therefore take the form

$$\mathcal{B}(\mu_0, \mu_b) = B_1(\mu_0)B_2(\mu_b). \tag{22}$$

Since $\mathcal{O}_{10}$ has no anomalous dimension above m_b and there is a common universal anomalous dimension for all the operators in $J_{\ell\ell}^{(0)}$ below m_b, there is a well-defined prescription for carrying this out. We take all contributions that cause perturbative corrections to $\mathcal{C}_{10a}$ and $\mathcal{C}_{10b}$ to be at the scale μ_b, so for this operator $B_1(\mu_0) = C_{10}$, and at one-loop order $B_2(\mu_b)$ includes $\alpha_s(\mu_b)\ln^2(\mu_b)$, $\alpha_s(\mu_b)\ln(\mu_b)$, and $\alpha_s(\mu_b)$ terms from matching the vertex diagram Fig. 2(b) and wave-function diagrams on to SCET. The analogous contributions from vertex diagrams for $\mathcal{C}_9$ and $\mathcal{C}_7$ are also matched at $\mu = \mu_b$ to determine their $B_2(\mu_b)$'s (for $\mathcal{C}_7$ the full-theory tensor current has a $\ln\mu$ that is matched at $\mu = \mu_0$). The universality of the anomalous dimensions in SCET guarantees that this procedure remains well-defined at any order in perturbation theory and can be organized into the product structure displayed in Eq. (22). For $\mathcal{C}_9$ and $\mathcal{C}_7$ there are additional non-vertex-like contributions that are matched on to $B_1(\mu_0)$ at a scale $\mu_0 \geq \mu_b$. These include contributions from four-quark operators $\mathcal{O}_{1-6}$ in the full theory, which will match on to $\mathcal{C}_9$ and $\mathcal{C}_7$ in SCET.

The difference between the full-theory diagram in Fig. 2(b) and the SCET graphs in Fig. 3(b) and 3(c) is IR finite (where we must use the same IR regulator in both theories, as is always the case for matching computations). In the UV the full-theory graph in Fig. 2(b) plus wave-function renormalization is μ-independent since the current is conserved. The graphs in SCET induce a μ dependence and an anomalous dimension for the effective-theory currents. These terms are matched at $\mu = \mu_b$. We start with the basis in Eq. (13) and find

$$\begin{aligned} C_{10a}(\mu_0, \mu_b) &= C_{10}\Big[1 + \frac{\alpha_s(\mu_b)}{\pi}\omega_a^V(s, \mu_b)\Big], \\ C_{10b,10c}(\mu_0, \mu_b) &= C_{10}\frac{\alpha_s(\mu_b)}{\pi}\omega_{b,c}^V(s), \end{aligned} \tag{23}$$

with a constant μ_0-independent C_{10}. The perturbative coefficients were computed in Ref. [27], and setting $\bar{n}\cdot p/m_b = (1-s)$ we find

$$\begin{aligned} \omega_a^V(s, \mu_b) &= -\frac{1}{3}\Big[2\ln^2(1-s) + 2\mathrm{Li}_2(s) \\ &\quad + \ln(1-s)\Big(\frac{1-3s}{s}\Big) + \frac{\pi^2}{12} + 6 + 2\ln^2\Big(\frac{\mu_b}{m_b}\Big) \\ &\quad + 5\ln\Big(\frac{\mu_b}{m_b}\Big) - 4\ln(1-s)\ln\Big(\frac{\mu_b}{m_b}\Big)\Big], \\ \omega_b^V(s) &= \frac{1}{3}\Big[\frac{2}{s} + \frac{2(1-s)}{s^2}\ln(1-s)\Big], \\ \omega_c^V(s) &= \frac{1}{3}\Big[\frac{(2s-1)(1-s)}{s^2}\ln(1-s) - \frac{(1-s)}{s}\Big]. \end{aligned} \tag{24}$$

For the matching on to $C_{9a,b,c}$ in the basis in Eq. (13) we have the same perturbative coefficients $\omega_{a,b,c}$ as for $C_{10a,b,c}$, because only the leptonic current differs:

$$\begin{aligned} C_{9a}(\mu_0, \mu_b) &= C_9^{\mathrm{mix}}(\mu_0)\Big[1 + \frac{\alpha_s(\mu_b)}{\pi}\omega_a^V(s, \mu_b)\Big], \\ C_{9b,9c}(\mu_0, \mu_b) &= C_9^{\mathrm{mix}}(\mu_0)\Big[\frac{\alpha_s(\mu_b)}{\pi}\omega_{b,c}^V(s)\Big]. \end{aligned} \tag{25}$$

However, for C_{9i} there are additional contributions, $C_9^{\mathrm{mix}}(\mu_0)$, from the matching at $\mu = \mu_0$, which at one-loop order and $\mathcal{O}(\alpha_s^0)$ includes Fig. 2(a):

$$\begin{aligned} C_9^{\mathrm{mix}}(\mu_0) &= C_9^{\mathrm{NDR}}(\mu_0) + \frac{2}{9}(3C_3 + C_4 + 3C_5 + C_6) - \frac{1}{2}h(1, s)(4C_3 + 4C_4 + 3C_5 + C_6) \\ &\quad + h\Big(\frac{m_c}{m_b}, s\Big)(3C_1 + C_2 + 3C_3 + C_4 + 3C_5 + C_6) - \frac{1}{2}h(0, s)(C_3 + 3C_4) + \frac{\alpha_s(\mu_0)}{\pi}C_9^{\mathrm{mix}(1)}(\mu_0), \end{aligned} \tag{26}$$

where all running coefficients on the RHS are $C_i = C_i(\mu_0)$. We shall discuss the relation of $C_9^{\rm mix}$ to $\tilde{C}_9^{\rm eff}$ in the local OPE analysis [10,11] after Eq. (33). In Eq. (26) the functions $h(1, s)$, $h(z, s)$, and $h(0, s)$ for the b-quark, c-quark, and light-quark penguin loops are [9,11]

$$h(z, s) = \frac{8}{9}\ln\left(\frac{\mu_0}{m_b}\right) - \frac{8}{9}\ln z + \frac{8}{27} + \frac{4}{9}\zeta - \frac{2}{9}(2+\zeta)\sqrt{|1-\zeta|} \times \left[\theta(1-\zeta)\left(-i\pi + \ln\frac{1+\sqrt{1-\zeta}}{1-\sqrt{1-\zeta}}\right) + \theta(\zeta-1)2\arctan\frac{1}{\sqrt{\zeta-1}}\right],$$

$$h(0, s) = \frac{8}{27} + \frac{8}{9}\ln\left(\frac{\mu_0}{m_b}\right) - \frac{4}{9}\ln s + \frac{4}{9}i\pi, \tag{27}$$

with $\zeta = 4z^2/s$. Higher-order $\mathcal{O}(\alpha_s)$ corrections in Eq. (26) are denoted by the $C_9^{\rm mix(1)}$ term. An important class of these corrections from mixing can be determined from the NNLL analysis in Refs. [13,14,16]:

$$C_9^{\rm mix(1)}(\mu_0) = C_8^{\rm NDR}\kappa_{8\to 9}(s, \mu_0) + C_1\kappa_{1\to 9}(s, \mu_0, \hat{m}_c) + C_2\kappa_{2\to 9}(s, \mu_0, \hat{m}_c). \tag{28}$$

To determine these terms one must be careful to separate out the factors in square brackets in Eq. (25). However we shall not attempt to include all NNLL terms consistently here. Contributions to $C_9^{\rm mix(1)}$ from the penguin coefficients $C_{3\text{–}6}$ are unknown but expected to be small (at the $\sim 1\%$ level).

Lastly, we turn to the results for C_{7i}. From the vertex graphs we have

$$C_{7a}(\mu_0, \mu_b) = C_7^{\rm mix}(\mu_0)\left[1 + \frac{\alpha_s(\mu_b)}{\pi}\omega_a^T(s, \mu_b)\right],$$
$$C_{7b,7c,7d}(\mu_0, \mu_b) = C_7^{\rm mix}(\mu_0)\frac{\alpha_s(\mu_b)}{\pi}\omega_{b,c,d}^T(s). \tag{29}$$

The ω_i^T perturbative corrections are again determined from the SCET matching in Ref. [27], which (switching to s) gives

$$\omega_a^T(s, \mu_b) = -\frac{1}{3}\left[2\ln^2(1-s) + 2\mathrm{Li}_2(s) + \ln(1-s)\left(\frac{2-4s}{s}\right) + \frac{\pi^2}{12} + 6 + 2\ln^2\left(\frac{\mu_b}{m_b}\right) + 5\ln\left(\frac{\mu_b}{m_b}\right) - 4\ln(1-s)\ln\left(\frac{\mu_b}{m_b}\right)\right],$$
$$\omega_b^T(s) = \omega_d^T(s) = 0,$$
$$\omega_c^T(s) = \frac{1}{3}\left[\frac{-2(1-s)\ln(1-s)}{s}\right]. \tag{30}$$

Additional contributions from other diagrams are matched at the scale μ_0 into $C_7^{\rm mix}(\mu_0)$. Note that, unlike the vector currents, the tensor current for O_7 gets renormalized for $\mu > m_b$, and we must include the corresponding $\ln(\mu_0/m_b)$ in $C_7^{\rm mix}(\mu_0)$, i.e.

$$C_7^{\rm mix}(\mu_0) = \frac{\bar{m}_b(\mu_0)}{m_B}\left\{C_7^{\rm NDR}(\mu_0)\left[1 - \frac{2\alpha_s(\mu_0)}{3\pi}\ln\left(\frac{\mu_0}{m_b}\right)\right] + \frac{\alpha_s(\mu_0)}{\pi}C_7^{\rm mix(1)}(\mu_0)\right\}, \tag{31}$$

where, much like in the case of $C_9^{\rm mix}$, we have

$$C_7^{\rm mix(1)}(\mu_0) = C_8^{\rm NDR}\kappa_a^8(s, \mu_0) + C_1\kappa_a^1(s, \mu_0, \hat{m}_c) + C_2\kappa_a^2(s, \mu_0, \hat{m}_c), \tag{32}$$

and the results for $\kappa_{8\to 7}(s, \mu_0)$, $\kappa_{1\to 7}(s, \mu_0, \hat{m}_c)$, and $\kappa_{2\to 7}(s, \mu_0, \hat{m}_c)$ can be found in Ref. [48]. Contributions to $C_7^{\rm mix(1)}$ from the penguin coefficients $C_{3\text{–}6}$ can be found in Ref. [49].

Using Eq. (20), $\bar{n}\cdot q n\cdot q/m_B^2 = y_H$, and $n\cdot q/m_B = 1 - u_H$, we can use the above results to give the final coefficients for our basis of operators with the minimal number of Dirac structures, namely

$$\begin{aligned}
\mathcal{C}_9 &= C_9^{\rm mix}(\mu_0)\left\{1 + \frac{\alpha_s(\mu_b)}{\pi}\left[\omega_a^V(s,\mu_b) + \frac{1}{2}\omega_b^V(s) + \frac{(1-u_H)^2\omega_c^V(s)}{(1-u_H)^2 - y_H}\right]\right\} \\
&\quad + C_7^{\rm mix}(\mu_0)\frac{\alpha_s(\mu_b)}{\pi}\left[\frac{2(1-u_H)[\omega_c^T(s) - \omega_d^T(s)]}{(1-u_H)^2 - y_H} - \frac{\omega_b^T(s)}{(1-u_H)}\right], \\
\mathcal{C}_7 &= C_7^{\rm mix}(\mu_0)\left\{1 + \frac{\alpha_s(\mu_b)}{\pi}\left[\omega_a^T(s,\mu_b) - \frac{1}{2}\omega_b^T(s) + \frac{y_H\omega_d^T(s) - (1-u_H)^2\omega_c^T(s)}{(1-u_H)^2 - y_H}\right]\right\} \\
&\quad - C_9^{\rm mix}(\mu_0)\frac{\alpha_s(\mu_b)}{\pi}\left[\frac{y_H\omega_b^V(s)}{4(1-u_H)} + \frac{y_H(1-u_H)\omega_c^V(s)}{2[(1-u_H)^2 - y_H]}\right], \\
\mathcal{C}_{10a} &= C_{10}\left\{1 + \frac{\alpha_s(\mu_b)}{\pi}\omega_a^V(s,\mu_b)\right\}, \\
\mathcal{C}_{10b} &= C_{10}\frac{\alpha_s(\mu_b)}{\pi}\left[\omega_b^V(s) + \frac{2(1-u_H)^2}{(1-u_H)^2 - y_H}\omega_c^V(s)\right],
\end{aligned} \tag{33}$$

where the terms have the structure of a sum over products $B_1(\mu_0)B_2(\mu_b)$, as desired.

In using the results in Eq. (33) one can choose to work to different orders in the μ_0- and μ_b-dependent terms, as shown in Eq. (3). For the μ_0 dependence, $C_9^{\rm mix}(\mu_0)$ and $C_7^{\rm mix}(\mu_0)$ include terms from matching at m_W and running to m_b, as well as matching contributions at m_b that cancel the μ_0 dependence from the other pieces. Thus, these coefficients have only a small residual μ_0 dependence, which is canceled at higher orders, just as in the local OPE. The $\mathcal{C}_i$ coefficients depend on μ_b, both through $\alpha_s(\mu_b)$ and through explicit μ_b dependence in ω_a^T and ω_a^V. The $\ln\mu_b$ dependence in ω_a^V and ω_a^T is identical, as expected from the known independence of the anomalous dimension on the Dirac structure in SCET. The μ_b dependence in $\mathcal{C}_i(\mu_b, \mu_0)$ is universal, and will cancel against the universal μ_b dependence in the jet and shape functions, which they multiply in the decay rates. We consider the phenomenological organization of the perturbative series for μ_0 and μ_b terms in turn.

First consider the μ_0 terms. Because of mixing, the sizes of contributions to $C_9^{\rm NDR}$ are comparable at LL and NLL orders [10,11], so a reasonable first approximation is to take the NLL result (just as for the local OPE decay rate). This entails dropping the $\mathcal{O}(\alpha_s)$ matching corrections $C_9^{\rm mix(1)}$ and $C_7^{\rm mix(1)}$, and running C_9 at NLL order with C_7 at LL order. As an improved approximation, we would then adopt the operationally well-defined NNLL approach [13] of running both C_9 and C_7 to NLL order and keeping the $\mathcal{O}(\alpha_s)$ matching corrections at m_b.[5]

Below m_b there are Sudakov logarithms. For the μ_b dependence, the RG evolution in SCET sums these double-logarithmic series. As a first approximation we could take the LL and NLL running in $U_H(\mu_b, \mu_i)$ and $U_S(\mu_i, \mu_\Lambda)$ in Eq. (3), while using tree-level matching for $B_2(\mu_b)$ and $\mathcal{J}(\mu_i)$. This is consistent because the NLL running is equivalent to LL running in a single-log resummation. As a second approximation we could then take NNLL running in both terms and include one-loop matching for both $B_2(\mu_b)$ and $\mathcal{J}(\mu_i)$. However since the scales $m_b^2 \gg m_b\Lambda \gg 1\ {\rm GeV}^2$ are not as well separated as $m_W^2 \gg m_b^2$, we could instead consider the second approximation to include the one-loop matching for $B_2(\mu_b)$ and $\mathcal{J}(\mu_i)$ with NLL running, but without including the full NNLL running (for which parts remain unknown).

Our procedure for split matching above was based on the nonrenormalization of $\mathcal{O}_{10}$ in QCD. It can also be thought of as matching in two steps. First one matches at μ_0 on to the scale-invariant operators

$$J^{(0)} = C_9^{\rm mix}(\bar{s}P_R\gamma^\mu b)(\bar{\ell}\gamma_\mu\ell) + C_{10}(\bar{s}P_R\gamma^\mu b)(\bar{\ell}\gamma_\mu\gamma_5\ell) - C_7^{\rm mix}\frac{2m_B q_\tau}{q^2}[(\bar{s}P_R i\sigma^{\mu\tau}b)(\mu = m_b)](\bar{\ell}\gamma_\mu\ell), \quad (34)$$

to determine the coefficients $C_{7,9}^{\rm mix}$. These coefficients are μ_0 independent at the order in perturbation theory to which the matching is done. Secondly, the operators in Eq. (34) are matched on to the SCET currents in Eq. (19) at the scale μ_b to determine the coefficients $\mathcal{C}_7$, $\mathcal{C}_9$, $\mathcal{C}_{10a,b}$. In Eq. (34) the operators for $C_9^{\rm mix}$ and C_{10} are conserved, but the tensor current has an anomalous dimension, and so we take $\mu = m_b$ as a reference point for matching on to a scale-invariant operator. This choice corresponds to the $\ln m_b$ factor in Eq. (31) for $C_7^{\rm mix}$. A different choice will affect the division of $\alpha_s(\mu_0)$ or $\alpha_s(\mu_b)$ terms. Note that Eq. (34) should be thought of only as an auxiliary step to facilitate the split matching; there is no sense in which the running of the tensor current is relevant by itself. In general the split-matching procedure could be carried out in a manner that gives different constant terms at a given order, but any such ambiguity will cancel order by order in $\mathcal{C}_7$ and $\mathcal{C}_9$ (and explicitly if $\mu_0 = \mu_b$).

Finally, note that our ω_a differs from the result for $\omega^{\rm OPE}$ identified in Ref. [11] for the partonic semileptonic decay rate when using the local OPE,

$$\omega_{\rm semi}^{\rm OPE} = -\frac{1}{3}\bigg[2\ln(s)\ln(1-s) + 4{\rm Li}_2(s) + \ln(1-s)\Big(\frac{5+4s}{1+2s}\Big) + \frac{2s(1+s)(1-2s)}{(1-s)^2(1+2s)}\ln(s) - \frac{(5+9s-6s^2)}{2(1-s)(1+2s)} + \frac{2\pi^2}{3}\bigg]. \quad (35)$$

Here $\omega_{\rm semi}^{\rm OPE}$ contains both vertex and bremsstrahlung contributions evaluated in the full theory. Grouping these contributions with the Wilson coefficient for $\mathcal{O}_9$ gives

$$C_9^{\rm local}(\mu) = C_9^{\rm mix}(\mu) + P_0^{\rm NDR}(\mu)\frac{\alpha_s(\mu)}{\pi}\omega_{\rm semi}^{\rm OPE}, \quad (36)$$

which is $\tilde{C}_9^{\rm eff}$ in the notation in Ref. [10]. At LO, the restricted phase space in the shape-function region causes bremsstrahlung to contribute only to the jet and shape functions, and not at the scale $\mu \simeq m_b$. The shape function and jet function also modify the contributions from the vertex graphs. Thus, instead of $\omega_{\rm semi}^{\rm OPE}$ the final results in the shape-function region are given by our ω_i^V and ω_i^T factors appearing in C_{9i} and C_{7i}. Consequently, the main difference is in the terms we match at $\mu = \mu_b$, while the terms matched at $\mu = \mu_0$ that appear in $C_9^{\rm mix}$ and $C_7^{\rm mix}$ are identical to terms appearing in the local OPE analysis.

B. RG evolution between μ_b and μ_i

The running of the Wilson coefficients in SCET from the scale $\mu_b^2 \sim m_b^2$ to $\mu_i^2 \sim m_b\Lambda_{\rm QCD}$ involves double Sudakov

[5] We assume that matching at the high scale, m_W, is always done at the order appropriate to the running of $U_W(\mu_W, \mu_0)$ in Eq. (3).

logarithms and was derived in Refs. [26,27] at NLL order. The SCET running is independent of the Dirac structure of the currents, which is a reflection of the spin symmetry structure of the current. We briefly outline a short argument for why this is true to all orders in perturbation theory. The leading-order currents in SCET have the structure

$$J = (\bar{\xi}_n W)_p \Gamma (Y^\dagger h_v), \tag{37}$$

and we wish to see that their anomalous dimension is independent of Γ. The anomalous dimensions are computed from the UV structure of SCET loop diagrams, with the Lagrangians in Eq. (9). Soft gluon loops involve contractions between the Wilson line $Y^\dagger$ and the h_v and do not change the Dirac structure. Next consider the collinear loops. The attachment of a gluon from the Wilson line W to the collinear quark gives a factor of a projection matrix, which can be pushed through $\gamma_\perp$'s to give $\bar{\xi}_n \bar{n}\!\!\!/ n\!\!\!/ /4 = \bar{\xi}_n$. Thus it does not modify the Dirac structure, so only insertions from the $iD\!\!\!\!/_c^\perp 1/(i\bar{n}\cdot D_c) iD\!\!\!\!/_c^\perp$ term are of concern. These terms give structures of the form $\bar{u}_n^{(u)} \gamma_\perp^{\mu_1}\gamma_\perp^{\mu_2}\cdots\gamma_\perp^{\mu_{2k}}\Gamma u_v^{(b)}$, where all μ_i indices are contracted with each other. Using $\{\gamma_\perp^\mu, \gamma_\perp^\nu\} = 2g_\perp^{\mu\nu}$ and $\gamma_\perp^\mu \gamma^\perp_\mu = d-2$ we can reduce this product to terms with zero $\gamma_\perp$'s since all vector indices are contracted. Hence all diagrams reduce to having the Dirac structure that was present at tree level, $\bar{u}_n^{(u)}\Gamma u_v^{(b)}$.

Thus, all the LO coefficients obey the same homogeneous anomalous dimension equation,

$$\begin{aligned}
\mu\frac{d}{d\mu}\mathcal{C}_i(\mu) &= \Big[-\Gamma_{\rm cusp}(\alpha_s)\ln\Big(\frac{\mu}{\bar{\mathcal{P}}}\Big) + \tilde{\gamma}(\alpha_s)\Big]\mathcal{C}_i(\mu) \\
&= \Big[-\Gamma_{\rm cusp}(\alpha_s)\ln\Big(\frac{\mu}{\mu_b}\Big) + \Big\{\tilde{\gamma}(\alpha_s) + \Gamma_{\rm cusp}(\alpha_s)\ln\Big(\frac{\bar{n}\cdot p}{\mu_b}\Big)\Big\}\Big]\mathcal{C}_i(\mu).
\end{aligned} \tag{38}$$

This must be integrated together with the beta function $\beta = \mu d/d\mu\, \alpha_s(\mu)$ to solve for U_H in

$$\mathcal{C}_i(\mu_i) = \sqrt{U_H(\mu_i, \mu_b)}\,\mathcal{C}_i(\mu_b). \tag{39}$$

In the second line of Eq. (38) we used the fact that $\bar{\mathcal{P}}$ gives the total partonic $\bar{n}\cdot p$ momentum of the jet X_s in the $B \to X_s \ell^+\ell^-$ matrix element, and we introduced artificial dependence on the matching scale μ_b in order to make the $\bar{n}\cdot p$ dependence appear in a small logarithm. Here $\bar{n}\cdot p = m_b - \bar{n}\cdot q$. We write

$$\Gamma^{\rm cusp} = \sum_{n=0}^{\infty}\Gamma_n^{\rm cusp}\Big(\frac{\alpha_s}{4\pi}\Big)^{n+1}, \qquad \tilde{\gamma} = \sum_{n=0}^{\infty}\tilde{\gamma}_n\Big(\frac{\alpha_s}{4\pi}\Big)^{n+1}, \qquad \beta = -2\alpha_s\sum_{n=0}^{\infty}\beta_n\Big(\frac{\alpha_s}{4\pi}\Big)^{n+1}. \tag{40}$$

At NLL order we need $\beta_0 = 11C_A/3 - 2n_f/3$, $\beta_1 = 34C_A^2/3 - 10C_A n_f/3 - 2C_F n_f$ and

$$\Gamma_0^{\rm cusp} = 4C_F, \qquad \Gamma_1^{\rm cusp} = 8C_F B = 8C_F\Big[C_A\Big(\frac{67}{18} - \frac{\pi^2}{6}\Big) - \frac{5}{9}n_f\Big], \qquad \tilde{\gamma}_0 = -5C_F, \tag{41}$$

where $C_A = 3$ and $C_F = 4/3$ for SU(3). For the number of active flavors we take $n_f = 4$ since we are running below m_b. The cusp anomalous dimension $\Gamma_1^{\rm cusp}$ was computed in Ref. [50], and the result for $\Gamma_2^{\rm cusp}$ was recently found in Ref. [51]. RG evolution in SCET at NNLL order has been considered in Refs. [44,52]. For the NNLL result one needs $\Gamma_2^{\rm cusp}$, $\tilde{\gamma}_1$, and β_2. For $\tilde{\gamma}_1$ an independent calculation does not exist, but a conjecture for its value was given in Ref. [44] based on the structure of the three-loop splitting function [51]. For the sake of clarity we stick to NLL order here. The result is

$$U_H(\mu_i, \mu_b) = \exp\Big[\frac{2g_0(r_1)}{\alpha_s(\mu_b)} + 2g_1(r_1, \bar{n}\cdot p)\Big], \tag{42}$$

where the independent variable is μ_i and

$$r_1(\mu_i) = \frac{\alpha_s(\mu_i)}{\alpha_s(\mu_b)} = \frac{2\pi}{2\pi + \beta_0\alpha_s(\mu_b)\ln(\mu_i/\mu_b)}, \tag{43}$$

with

$$\begin{aligned}
g_0(r_1) &= -\frac{4\pi C_F}{\beta_0^2}\Big[\frac{1}{r_1} - 1 + \ln r_1\Big], \\
g_1(r_1, \bar{n}\cdot p) &= -\frac{C_F\beta_1}{\beta_0^3}\Big[1 - r_1 + r_1\ln r_1 - \frac{1}{2}\ln^2 r_1\Big] \\
&\quad + \frac{C_F}{\beta_0}\Big[\frac{5}{2} - 2\ln\Big(\frac{\bar{n}\cdot p}{\mu_b}\Big)\Big]\ln r_1 \\
&\quad - \frac{2C_F B}{\beta_0^2}[r_1 - 1 - \ln r_1].
\end{aligned} \tag{44}$$

This is the form for the universal running of the LO SCET currents found in Ref. [27]. Switching to $\alpha_s(\mu_i)$ as the independent variable, with $r_1 = \alpha_s(\mu_i)/\alpha_s(\mu_b)$, gives

$$U_H(\mu_i, \mu_b) = \left(\frac{\bar{n}\cdot p}{\mu_b}\right)^{-(4C_F/\beta_0)\ln r_1} \exp\left[\frac{2g_0(r_1)}{\alpha_s(\mu_b)} + 2\tilde{g}_1(r_1)\right], \tag{45}$$

where $g_0(r_1)$ is as in Eq. (44) and

$$\tilde{g}_1(r_1) = \frac{C_F\beta_1}{2\beta_0^3}\ln^2 r_1 + \frac{5C_F}{2\beta_0}\ln r_1 + \frac{C_F}{\beta_0^3}(2B\beta_0 - \beta_1)(1 - r_1 + \ln r_1). \tag{46}$$

This form of the evolution with $\alpha_s(\mu)$ as the variable was used in Ref. [34], and is also the one we adopt here. The decay rate is computed from a time-ordered product of currents and so at the intermediate scale $\mu_i^2 \sim m_b\Lambda$ will involve products

$$\mathcal{C}_i(\mu_i, \mu_0)\mathcal{C}_j(\mu_i, \mu_0) = U_H(\mu_i, \mu_b)\mathcal{C}_i(\mu_b, \mu_0)\mathcal{C}_j(\mu_b, \mu_0), \tag{47}$$

explaining why we used a notation with $\sqrt{U_H}$ in Eq. (39).

C. Hadronic tensor and decay rates

In the last two sections we constructed the required basis of SCET current operators with matching at $\mu_0^2 \sim \mu_b^2 \sim m_b^2$ and evolution to $\mu_i^2 \sim m_b\Lambda$. At the scale μ_i we take time-ordered products of the SCET currents and compute the decay rates using the optical theorem. In this section we discuss the tensor decomposition of the time-ordered products and results for differential decay rates.

In order to simplify the computation of decay rates it is useful to write the sum of hadronic operators as a sum of left-handed and right-handed terms since for massless leptons we have only LL or RR contributions [20]. Doing this for our current, we have

$$\begin{aligned}\mathcal{J}_{\ell\ell}^{(0)} &= [\mathcal{C}_9 - \mathcal{C}_{10a}](\bar{\chi}_n\gamma_\mu P_L\mathcal{H}_v)(\bar{\ell}\gamma^\mu P_L\ell) + [\mathcal{C}_9 + \mathcal{C}_{10a}](\bar{\chi}_n\gamma_\mu P_L\mathcal{H}_v)(\bar{\ell}\gamma^\mu P_R\ell) + \mathcal{C}_{10b}(\bar{\chi}_n v_\mu P_R\mathcal{H}_v)(\bar{\ell}\gamma^\mu\gamma_5\ell) \\ &\quad - \mathcal{C}_7\frac{2m_B q^\tau}{q^2}(\bar{\chi}_n i\sigma_{\mu\tau}\mathcal{H}_v)(\bar{l}\gamma^\mu l) \\ &= (J_{L\mu}L_L^\mu + J_{R\mu}L_R^\mu),\end{aligned} \tag{48}$$

where

$$L_L^\mu = \bar{\ell}\gamma^\mu P_L\ell, \qquad L_R^\mu = \bar{\ell}\gamma^\mu P_R\ell, \qquad J_{L(R)}^\mu = \bar{\chi}_n P_R\left[(\mathcal{C}_9 \mp \mathcal{C}_{10a})\gamma^\mu + \mathcal{C}_7\frac{2m_B\gamma^\mu\not{q}}{q^2} \mp \mathcal{C}_{10b}v^\mu\right]\mathcal{H}_v \equiv \bar{\chi}_n\Gamma_{L(R)}^\mu\mathcal{H}_v. \tag{49}$$

Thus, the inclusive decay rate for $\bar{B} \to X_s\ell^+\ell^-$ is proportional to $(W_{\mu\nu}^L L_L^{\mu\nu} + W_{\mu\nu}^R L_R^{\mu\nu})$, where the leptonic parts $L_{L(R)}^{\mu\nu}$ and hadronic parts $W_{L(R)}^{\mu\nu}$ are given by

$$L_{L(R)}^{\mu\nu} = \sum_{\rm spin}[\bar{l}_{L(R)}(p_+)\gamma^\mu l_{L(R)}(p_-)][\bar{l}_{L(R)}(p_-)\gamma^\nu l_{L(R)}(p_+)] = 2[p_+^\mu p_-^\nu + p_-^\mu p_+^\nu - g^{\mu\nu}p_+\cdot p_- \mp i\epsilon^{\mu\nu\alpha\beta}p_{+\alpha}p_{-\beta}], \tag{50}$$

and

$$\begin{aligned}W_{\mu\nu}^{L(R)} &= \frac{1}{2m_B}\sum_X(2\pi)^3\delta^4(p_B - q - p_X)\langle\bar{B}|J_\mu^{L(R)\dagger}|X\rangle\langle X|J_\nu^{L(R)}|\bar{B}\rangle \\ &= -g_{\mu\nu}W_1^{L(R)} + v_\mu v_\nu W_2^{L(R)} + i\epsilon_{\mu\nu\alpha\beta}v^\alpha q^\beta W_3^{L(R)} + q_\mu q_\nu W_4^{L(R)} + (v_\mu q_\nu + v_\nu q_\mu)W_5^{L(R)}.\end{aligned} \tag{51}$$

Here, we use relativistic normalization for the $|\bar{B}\rangle$ states. For convenience, we define projection tensors $P_i^{\mu\nu}$ so that

$$W_i^{L(R)} = P_i^{\mu\nu}W_{\mu\nu}^{L(R)}. \tag{52}$$

They are

$$\begin{aligned}&P_1^{\mu\nu} = -\frac{1}{2}g^{\mu\nu} + \frac{q^2v^\mu v^\nu + q^\mu q^\nu - v\cdot q(v^\mu q^\nu + v^\nu q^\mu)}{2[q^2 - (v\cdot q)^2]}, \qquad P_2^{\mu\nu} = \frac{3q^2P_1^{\mu\nu} + q^2g^{\mu\nu} - q^\mu q^\nu}{[q^2 - (v\cdot q)^2]}, \\ &P_3^{\mu\nu} = \frac{-i\epsilon^{\mu\nu\alpha\beta}q_\alpha v_\beta}{2[q^2 - (v\cdot q)^2]}, \qquad P_4^{\mu\nu} = \frac{g^{\mu\nu} - v^\mu v^\nu + 3P_1^{\mu\nu}}{[q^2 - (v\cdot q)^2]}, \qquad P_5^{\mu\nu} = \frac{g^{\mu\nu} + 4P_1^{\mu\nu} - P_2^{\mu\nu} - q^2P_4^{\mu\nu}}{2v\cdot q}.\end{aligned} \tag{53}$$

The optical theorem relates $W_{\mu\nu}^{L(R)}$ to the forward-scattering amplitude defined as

$$T^L_{\mu\nu} = \frac{-i}{2m_B}\int d^4x e^{-iq\cdot x}\langle \bar{B}|TJ^{L\dagger}_\mu(x)J^L_\nu(0)|\bar{B}\rangle = -g_{\mu\nu}T^L_1 + v_\mu v_\nu T^L_2 + i\epsilon_{\mu\nu\alpha\beta}v^\alpha q^\beta T^L_3 + q_\mu q_\nu T^L_4 + (v_\mu q_\nu + v_\nu q_\mu)T^L_5, \tag{54}$$

with an analogous definition for $T^R_{\mu\nu}$, giving

$$W^L_i = -\frac{1}{\pi}\,\mathrm{Im}T^L_i, \qquad W^R_i = -\frac{1}{\pi}\,\mathrm{Im}T^R_i. \tag{55}$$

Contracting the lepton tensor $L^{\mu\nu}_{L(R)}$ with $W^{\mu\nu}_{L(R)}$ and neglecting the mass of the leptons give the differential decay rate

$$\frac{d^3\Gamma}{dq^2dE_-dE_+} = \Gamma_0\frac{96}{m_B^5}[q^2W_1 + (2E_-E_+ - q^2/2)W_2 + q^2(E_- - E_+)W_3]\theta(4E_-E_+ - q^2), \tag{56}$$

where $E_\pm = v\cdot p_\pm$, $W_1 = W^L_1 + W^R_1$, $W_2 = W^L_2 + W^R_2$, $W_3 = W^L_3 - W^R_3$ and the normalization factor is

$$\Gamma_0 = \frac{G_F^2m_B^5}{192\pi^3}\frac{\alpha^2}{16\pi^2}|V_{tb}V^*_{ts}|^2. \tag{57}$$

The W_i are functions of q^2 and $v\cdot q = v\cdot(p_+ + p_-)$. Another quantity of interest is the forward-backward asymmetry in the variable

$$\cos\theta = \frac{v\cdot p_- - v\cdot p_+}{\sqrt{(v\cdot q)^2 - q^2}}, \tag{58}$$

where θ is the angle between the B and ℓ^+ in the CM frame of the $\ell^+\ell^-$ pair:

$$\frac{d^2A_{\rm FB}}{dv\cdot q dq^2} \equiv \int_{-1}^{1} d(\cos\theta)\frac{\mathrm{sign}(\cos\theta)}{\Gamma_0}\frac{d^3\Gamma}{dv\cdot q dq^2 d\cos\theta} = \frac{48q^2}{m_B^5}[(v\cdot q)^2 - q^2]W_3. \tag{59}$$

In terms of the dimensionless variables

$$x_H = \frac{2E_{\ell^-}}{m_B}, \qquad \bar{y}_H = \frac{\bar{n}\cdot p_X}{m_B}, \qquad u_H = \frac{n\cdot p_X}{m_B}, \tag{60}$$

the triply differential decay rate is

$$\frac{1}{\Gamma_0}\frac{d^3\Gamma}{dx_Hd\bar{y}_Hdu_H} = 24m_B(\bar{y}_H - u_H)\bigg\{(1-u_H)(1-\bar{y}_H)W_1 + \frac{1}{2}(1-x_H-u_H)(x_H+\bar{y}_H-1)W_2 + \frac{m_B}{2}(1-u_H)(1-\bar{y}_H)(2x_H+u_H+\bar{y}_H-2)W_3\bigg\}, \tag{61}$$

where $W_i = W_i(u_H, \bar{y}_H)$. For a strict SCET expansion we want $n\cdot p_X \ll \bar{n}\cdot p_X$ i.e. $u_H \ll \bar{y}_H$. However, it is useful to keep the full dependence on the phase-space prefactors rather than expanding them, because it is then simpler to make contact with the total rate in the local OPE, as emphasized recently in Refs. [53,54], and so we keep these factors here. We shall also keep the formally subleading kinematic prefactors in our hard functions rather than expanding them as we did in Ref. [38]. Other variables of interest include the dilepton and hadronic invariant masses,

$$y_H = \frac{q^2}{m_B^2}, \qquad s_H = \frac{m_X^2}{m_B^2}, \tag{62}$$

where

$$s_H = u_H\bar{y}_H, \qquad y_H = (1-u_H)(1-\bar{y}_H), \tag{63}$$

so that $[\bar{y}_H \ge u_H]$

$$\{\bar{y}_H, u_H\} = \frac{1}{2}[1 - y_H + s_H \pm \sqrt{(1-y_H+s_H)^2 - 4s_H}]. \tag{64}$$

A few interesting doubly differential spectra are

$$\frac{1}{\Gamma_0}\frac{d^2\Gamma}{d\bar{y}_Hdu_H} = 24m_B(\bar{y}_H-u_H)^2\bigg\{(1-u_H)(1-\bar{y}_H)W_1 + \frac{1}{12}(\bar{y}_H-u_H)^2W_2\bigg\},$$

$$\frac{1}{\Gamma_0}\frac{d^2\Gamma}{dy_Hds_H} = 2m_B\sqrt{(1-y_H+s_H)^2-4s_H}\times\{12y_HW_1 + [(1-y_H+s_H)^2-4s_H]W_2\},$$

$$\frac{1}{\Gamma_0}\frac{d^2\Gamma}{dy_Hdu_H} = \frac{2m_B}{(1-u_H)^3}[(1-u_H)^2-y_H]^2\times\bigg\{12y_HW_1 + \bigg[\frac{(1-u_H)^2-y_H}{(1-u_H)}\bigg]^2W_2\bigg\},$$

$$\frac{1}{\Gamma_0}\frac{d^2\Gamma}{ds_Hdu_H} = \frac{2m_B(s_H-u_H^2)^2}{u_H^5}\{12u_H(1-u_H)(u_H-s_H)W_1 + (s_H-u_H^2)^2W_2\}. \tag{65}$$

For doubly differential forward-backward asymmetries we find

$$\frac{d^2A_{\rm FB}}{d\bar{y}_H du_H} = 6m_B^2(\bar{y}_H - u_H)^3(1-u_H)(1-\bar{y}_H)W_3,$$
$$\frac{d^2A_{\rm FB}}{dy_H ds_H} = 6m_B^2 y_H[(1-y_H+s_H)^2 - 4s_H]W_3,$$
$$\frac{d^2A_{\rm FB}}{dy_H du_H} = 6m_B^2\frac{y_H[(1-u_H)^2-y_H]^3}{(1-u_H)^4}W_3, \qquad (66)$$
$$\frac{d^2A_{\rm FB}}{ds_H du_H} = 6m_B^2\frac{(s_H-u_H^2)^3(u_H-s_H)(1-u_H)}{u_H^5}W_3.$$

D. LO matrix elements in SCET

At lowest order in the Λ/m_b expansion, the only time-ordered product consists of two lowest-order currents $\mathcal{J}_{\ell\ell}^{(0)}$ as shown in Fig. 4. The factorization of hard contributions into the SCET Wilson coefficients and the decoupling of soft and collinear gluons at lowest order are identical to the steps for $B\to X_s\gamma$ and $B\to X_u\ell\bar{\nu}$, and directly give the factorization theorem for these time-ordered products [29]. The SCET result agrees with the factorization theorem of Korchemsky and Sterman [31]. However, the structure of $\alpha_s(\sqrt{m_b\Lambda})$ and $\alpha_s(m_b)$ corrections differs from the parton-model rate, as mentioned in Refs. [33,34]. Beyond lowest order in $\alpha_s(m_b)$ the kinematic dependences also differ, as mentioned in Ref. [38]. For $B\to X_u\ell\bar{\nu}$, the final triply differential rate with perturbative corrections at $\mathcal{O}(\alpha_s)$ can be found in Refs. [33,34].

The factorization and use of the optical theorem is carried out at the scale $\mu=\mu_i$, and we expand $W_i = W_i^{(0)} + W_i^{(2)} + \ldots$ in powers of $\lambda = (\Lambda_{\rm QCD}/m_b)^{1/2}$ (with no linear term). For $B\to X_s\ell^+\ell^-$ we have bilinear hadronic current operators in SCET in Eq. (19) and so, as is the case for $B\to X_u\ell\bar{\nu}$, we find

$$W_i^{(0)} = h_i(p_X^+, p_X^-, \mu_i)\int_0^{p_X^+} dk^+\,\mathcal{J}^{(0)}(p^-, k^+, \mu_i) \times f^{(0)}(k^+ + \bar{\Lambda} - p_X^+, \mu_i). \qquad (67)$$

This result is important, since it states that the same shape function $f^{(0)}$ appears in $B\to X_s\ell^+\ell^-$ as appears in $B\to X_s\gamma$ and $B\to X_u\ell\bar{\nu}$. This formula relies on the power counting $s\sim y_H\sim\lambda^0$ that we adopted (and would not be true for the counting $s\sim\lambda^2$ discussed in Appendix B). At tree level the structure of this factorization theorem is illustrated by Fig. 4. The hard coefficients here are

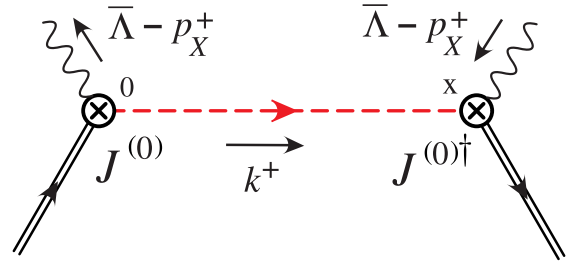

FIG. 4 (color online). Time-ordered product for the leading-order factorization theorem.

$$h_1(p_X^+, p_X^-, \mu_i) = \frac{1}{4}\,{\rm Tr}[P_v\bar{\Gamma}_\mu^L \not{\bar{n}} \Gamma_\nu^L]P_1^{\mu\nu} + \frac{1}{4}\,{\rm Tr}[P_v\bar{\Gamma}_\mu^R \not{\bar{n}} \Gamma_\nu^R]P_1^{\mu\nu},$$
$$h_2(p_X^+, p_X^-, \mu_i) = \frac{1}{4}\,{\rm Tr}[P_v\bar{\Gamma}_\mu^L \not{\bar{n}} \Gamma_\nu^L]P_2^{\mu\nu} + \frac{1}{4}\,{\rm Tr}[P_v\bar{\Gamma}_\mu^R \not{\bar{n}} \Gamma_\nu^R]P_2^{\mu\nu}, \qquad (68)$$
$$h_3(p_X^+, p_X^-, \mu_i) = \frac{1}{4}\,{\rm Tr}[P_v\bar{\Gamma}_\mu^L \not{\bar{n}} \Gamma_\nu^L]P_3^{\mu\nu} - \frac{1}{4}\,{\rm Tr}[P_v\bar{\Gamma}_\mu^R \not{\bar{n}} \Gamma_\nu^R]P_3^{\mu\nu},$$

with $P_v = (1+\not{v})/2$ and $\bar{\Gamma} = \gamma^0\Gamma^\dagger\gamma^0$. In Eq. (67) we have the same leading-order shape function as in $B\to X_s\gamma$ and $B\to X_u\ell\bar{\nu}$, namely

$$f^{(0)}(\ell^+, \mu_i) = \frac{1}{2}\int\frac{dx^-}{4\pi}e^{-ix^-\ell^+/2}\langle\bar{B}_v|\bar{\mathcal{H}}_v(\tilde{x})\mathcal{H}_v(0)|\bar{B}_v\rangle = \frac{1}{2}\langle\bar{B}_v|\bar{h}_v\delta(\ell^+ - in\cdot D)h_v|\bar{B}_v\rangle, \qquad (69)$$

where $\tilde{x}^\mu = \bar{n}\cdot x n^\mu/2$. This function was first discussed in Ref. [24]. The jet function is defined by $\mathcal{J}^{(0)}(p^-, k^+) = (-1/\pi)\,{\rm Im}\mathcal{J}_{\omega=p^-}^{(0)}(k^+)\times\theta(p_X^+ - k^+)$, where

$$i\left\langle 0\left| T\left[\bar{\chi}_{n,\omega}(0)\frac{\not{\bar{n}}}{4N_c}\chi_{n,\omega'}(x)\right]\right|0\right\rangle = \delta(\omega-\omega')\delta^2(x_\perp)\delta(x^+)\int\frac{dk^+}{2\pi}e^{-ik^+x^-/2}\mathcal{J}_\omega^{(0)}(k^+), \qquad (70)$$

and is known at one-loop order [33,34], namely

$$\mathcal{J}^{(0)}(p^-, zp_X^+, \mu_i) = \frac{1}{p_X^+}\left\{\delta(z)\left[1 + \frac{\alpha_s(\mu_i)C_F}{4\pi}\left(2\ln^2\frac{p^-p_X^+}{\mu_i^2} - 3\ln\frac{p^-p_X^+}{\mu_i^2} + 7 - \pi^2\right)\right] + \frac{\alpha_s(\mu_i)C_F}{4\pi}\left[\left(\frac{4\ln z}{z}\right)_+ + \left(4\ln\frac{p^-p_X^+}{\mu_i^2} - 3\right)\frac{1}{(z)_+}\right]\theta(z)\right\}\theta(1-z), \qquad (71)$$

where $z = k^+/p_X^+$. Despite appearances, only the combination zp_X^+ appears in $\mathcal{J}^{(0)}$ apart from the $\theta(1-z)$. This last θ function is induced by the soft function and, when one takes the imaginary part of the full time-ordered product, affects the complex structure. Therefore, we include it in our definition of $\mathcal{J}^{(0)}(p^-, k^+)$.

E. RG evolution between μ_Λ and μ_i

The function $f^{(0)}$ cannot be computed in perturbation theory and must therefore be extracted from data. This same function appears at LO in the $B \to X_s\gamma$, $B \to X_u \ell \bar{\nu}$ and $B \to X_s \ell^+\ell^-$ decay rates. In practice, a model for $f^{(0)}$ is written down with a few parameters, which are fitted to the data. The support of $f^{(0)}(\bar{\Lambda} - r^+)$ is $-\infty$ to $\bar{\Lambda}$ since $r^+ \in [0, \infty)$. It is often convenient to switch variables to $\hat{f}^{(0)}(r^+) = f^{(0)}(\bar{\Lambda} - r^+)$ which has support from 0 to ∞, although we shall keep using $f^{(0)}$ here. A typical three-parameter model is [36,53]

$$f^{(0)}(\bar{\Lambda} - r^+, \mu_\Lambda) = \hat{f}^{(0)}(r^+, \mu_\Lambda) = \frac{a^b (r^+)^{b-1}}{\Gamma(b) L^b} \exp\left(\frac{-ar^+}{L}\right)\theta(r^+), \quad (72)$$

where a, b are dimensionless and $L \sim \Lambda_{\rm QCD}$. These parameters can be fitted to the $B \to X_s\gamma$ photon spectrum and the function $f^{(0)}$ can then be used elsewhere. The most natural scale to fix this model at is $\mu = \mu_\Lambda \sim 1$ GeV, at which it contains no large logarithms. The result of evolving the shape function to the intermediate scale is then [34]

$$f^{(0)}(\bar{\Lambda} - r^+, \mu_i) = e^{V_S(\mu_i, \mu_\Lambda)} \frac{1}{\Gamma(\eta)} \times \int_0^{r^+} dr^{+\prime} \frac{f^{(0)}(\bar{\Lambda} - r^{+\prime}, \mu_\Lambda)}{\mu_\Lambda^\eta (r^+ - r^{+\prime})^{1-\eta}}. \quad (73)$$

(The structure of this result also applies at higher orders in RG-improved perturbation theory [44], and at one-loop order a similar structure was considered earlier, in Ref. [55].) At NLL order

$$\begin{aligned} V_S(\mu_i, \mu_\Lambda) = {}& \frac{\Gamma_0^{\rm cusp}}{2\beta_0^2}\left[\frac{-4\pi}{\alpha_s(\mu_\Lambda)}(r_2 - 1 - \ln r_2) + \frac{\beta_1}{2\beta_0}\ln^2 r_2 + \left(\frac{\Gamma_1^{\rm cusp}}{\Gamma_0^{\rm cusp}} - \frac{\beta_1}{\beta_0}\right)\left(1 - \frac{1}{r_2} - \ln r_2\right)\right] \\ & - \frac{\Gamma_0^{\rm cusp}}{\beta_0}\gamma_E \ln r_2 - \frac{\gamma_0}{\beta_0}\ln r_2, \quad (74) \\ \eta = {}& \frac{\Gamma_0^{\rm cusp}}{\beta_0}\ln r_2. \end{aligned}$$

Here, $r_2 = \alpha_s(\mu_\Lambda)/\alpha_s(\mu_i)$, $\Gamma_0^{\rm cusp}$ and $\Gamma_1^{\rm cusp}$ are the same as in Sec. II B and $\gamma_0 = -2C_F$. For numerical integration this can be rewritten in the form

$$f^{(0)}(\bar{\Lambda} - r^+, \mu_i) = e^{V_S(\mu_i, \mu_\Lambda)} \frac{1}{\Gamma(1+\eta)}\left(\frac{r^+}{\mu_\Lambda}\right)^\eta \times \int_0^1 dt f^{(0)}(\bar{\Lambda} - r^+(1 - t^{1/\eta}), \mu_\Lambda). \quad (75)$$

III. $B \to X_s \ell^+\ell^-$ SPECTRA IN THE SHAPE-FUNCTION REGION

A. Triply differential spectrum

At lowest order in the power expansion, Eqs. (53) and (67) give the result

$$W_i^{(0)} = h_i(p_X^-, p_X^+, m_b, \mu_i) \int_0^{p_X^+} dk^+ \mathcal{J}^{(0)}(p^-, k^+, \mu_i) \times f^{(0)}(k^+ + \bar{\Lambda} - p_X^+, \mu_i), \quad (76)$$

where RG evolution from the hard scale to the intermediate scale gives

$$h_i(p_X^-, p_X^+, \mu_i) = U_H(\mu_i, \mu_b) h_i(p_X^-, p_X^+, \mu_b), \quad (77)$$

and the results at $\mu = \mu_b$ are determined from the traces in Eq. (68):

$$\begin{aligned} h_1(p_X^-, p_X^+, \mu_b) &= \frac{1}{2}(|\mathcal{C}_9|^2 + |\mathcal{C}_{10a}|^2) + \frac{2\,{\rm Re}[\mathcal{C}_7\mathcal{C}_9^*]}{(1-\bar{y}_H)} + \frac{2|\mathcal{C}_7|^2}{(1-\bar{y}_H)^2}, \\ h_2(p_X^-, p_X^+, \mu_b) &= \frac{2(1-u_H)}{(\bar{y}_H - u_H)}(|\mathcal{C}_9|^2 + |\mathcal{C}_{10a}|^2 + {\rm Re}[\mathcal{C}_{10a}\mathcal{C}_{10b}^*]) + \frac{|\mathcal{C}_{10b}|^2}{2} - \frac{8|\mathcal{C}_7|^2}{(1-\bar{y}_H)(\bar{y}_H - u_H)}, \quad (78) \\ h_3(p_X^-, p_X^+, \mu_b) &= \frac{-4\,{\rm Re}[\mathcal{C}_{10a}\mathcal{C}_7^*]}{m_B(1-\bar{y}_H)(\bar{y}_H - u_H)} - \frac{2\,{\rm Re}[\mathcal{C}_{10a}\mathcal{C}_9^*]}{m_B(\bar{y}_H - u_H)}. \end{aligned}$$

Here $\mathcal{C}_i = \mathcal{C}_i(p_X^-, p_X^+, \mu_b, \mu_0, m_b)$, so these hard coefficients also depend on m_b and have residual μ_0 scale dependence. Explicit formulas are given in Eq. (33). For convenience we define

$$F^{(0)}(p_X^+, p_X^-) = U_H(\mu_i, \mu_b)\int_0^{p_X^+} dk^+ \mathcal{J}^{(0)}(p^-, k^+, \mu_i) f^{(0)}(k^+ + \bar{\Lambda} - p_X^+, \mu_i)$$
$$= p_X^+ U_H(\mu_i, \mu_b)\int_0^1 dz \mathcal{J}^{(0)}(p^-, z p_X^+, \mu_i) f^{(0)}(\bar{\Lambda} - p_X^+(1-z), \mu_i). \quad (79)$$

where $p_X^- = p^- + \bar{\Lambda}$. In terms of this function,

$$W_i^{(0)} = h_i(p_X^+, p_X^-, \mu_b) F^{(0)}(p_X^+, p_X^-). \quad (80)$$

We find that to NLL order

$$F^{(0)}(p_X^+, p_X^-) = U_H(\mu_i, \mu_b) f^{(0)}(\bar{\Lambda} - p_X^+, \mu_i) + U_H(\mu_i, \mu_b)\frac{\alpha_s(\mu_i) C_F}{4\pi}\bigg\{\bigg(2\ln^2\frac{p^- p_X^+}{\mu_i^2} - 3\ln\frac{p^- p_X^+}{\mu_i^2} + 7 - \pi^2\bigg)$$
$$\times f^{(0)}(\bar{\Lambda} - p_X^+, \mu_i) + \int_0^1 \frac{dz}{z}\bigg[4\ln\frac{z p^- p_X^+}{\mu_i^2} - 3\bigg][f^{(0)}(\bar{\Lambda} - p_X^+(1-z), \mu_i) - f^{(0)}(\bar{\Lambda} - p_X^+, \mu_i)]\bigg\}. \quad (81)$$

Note that, until we include the α_s corrections from the jet function, $F^{(0)}$ is independent of p_X^-, so that all of this dependence is in the $h_i(p_X^+, p_X^-, \mu_b)$ functions.

Now, the triply differential decay rate in Eq. (61) becomes

$$\frac{1}{\Gamma_0}\frac{d^3\Gamma}{dx_H d\bar{y}_H du_H} = 24 m_B(\bar{y}_H - u_H)\bigg\{(1-u_H)(1-\bar{y}_H)h_1 + \frac{1}{2}(1 - x_H - u_H)(x_H + \bar{y}_H - 1)h_2$$
$$+ \frac{m_B}{2}(1-u_H)(1-\bar{y}_H)(2x_H + u_H + \bar{y}_H - 2)h_3\bigg\} F^{(0)}(m_B u_H, m_B \bar{y}_H), \quad (82)$$

with $h_{1,2,3}$ from Eq. (78). As a check on this result, one can make the substitutions

$$\mathcal{C}_{9a} = -\mathcal{C}_{10a} = 1/2, \qquad \mathcal{C}_7 = \mathcal{C}_{10b} = 0,$$
$$\frac{G_F \alpha}{\sqrt{2}\pi} V_{tb} V_{ts}^* \to \frac{4 G_F}{\sqrt{2}} V_{ub}, \quad (83)$$

after which the h_1 and h_2 terms in Eq. (82) agree with terms in the leading-order shape-function spectrum for $B \to X_u \ell \bar{\nu}$ [33,56]. The h_3 term for $B \to X_s \ell\ell$ was the difference of products of left- and right-handed currents and so should not agree in this limit.

B. $d^2\Gamma/dq^2 dm_X^2$ spectrum with q^2 and m_X cuts

Next we discuss doubly differential rates and forward-backward asymmetries. For $d^2\Gamma/dq^2 dm_X^2$ the rate is obtained from Eq. (82) by integrating over x_H and changing variables. In terms of dimensionless variables $y_H = q^2/m_B^2$ and $s_H = m_X^2/m_B^2$ we have

$$\frac{1}{\Gamma_0}\frac{d^2\Gamma}{dy_H ds_H} = H^{ys}(y_H, s_H) m_B F^{(0)}(m_B u_H(y_H, s_H), m_B \bar{y}_H(y_H, s_H)),$$
$$\frac{1}{\Gamma_0}\frac{d^2 A_{\rm FB}}{dy_H ds_H} = K^{ys}(y_H, s_H) m_B F^{(0)}(m_B u_H(y_H, s_H), m_B \bar{y}_H(y_H, s_H)), \quad (84)$$

where

$$H^{ys}(y_H, s_H) = 2\sqrt{(1 - y_H + s_H)^2 - 4 s_H}\{12 y_H h_1 + [(1 - y_H + s_H)^2 - 4 s_H] h_2\},$$
$$K^{ys}(y_H, s_H) = 6 y_H[(1 - y_H + s_H)^2 - 4 s_H] h_3 \quad (85)$$

and we need to substitute $h_{1,2,3}$ from Eq. (78) and $u_H(y_H, s_H)$ and $\bar{y}_H(y_H, s_H)$, as given in Eq. (64). When one takes experimental cuts on q^2 and m_X^2,

$$y_H^{\min} < y_H < y_H^{\max}, \qquad 0 < s_H < s_H^0, \quad (86)$$

the limits on the doubly differential rate and forward-backward asymmetry in Eq. (84) are

$$1) \quad y_H^{\min} \le y_H \le y_H^{\max}, \qquad 0 \le s_H \le \min\{s_H^0, (1 - \sqrt{y_H})^2\},$$
$$2) \quad 0 \le s_H \le s_H^0, \qquad y_H^{\min} \le y_H \le \min\{y_H^{\max}, (1 - \sqrt{s_H})^2\}, \quad (87)$$

depending on the desired order of integration.

C. $d^2\Gamma/dm_X^2 dp_X^+$ spectrum with q^2 and m_X cuts

The hadronic invariant-mass spectrum and forward-backward asymmetry can be obtained by integrating the doubly differential spectra

$$\frac{1}{\Gamma_0}\frac{d^2\Gamma}{ds_H du_H} = H^s(s_H, u_H) m_B F^{(0)}\Big(m_B u_H, m_B \frac{s_H}{u_H}\Big), \qquad \frac{1}{\Gamma_0}\frac{d^2 A_{\rm FB}}{ds_H du_H} = K^s(s_H, u_H) m_B F^{(0)}\Big(m_B u_H, m_B \frac{s_H}{u_H}\Big) \tag{88}$$

over u_H. Here

$$\begin{aligned} H^s(s_H, u_H) &= \frac{4(s_H - u_H^2)^2}{(u_H - s_H)u_H^4}\Big\{(1-u_H)(u_H - s_H)(3u_H - 2s_H - u_H^2)(|\mathcal{C}_9|^2 + |\mathcal{C}_{10a}|^2) + 4u_H(3u_H - s_H - 2u_H^2)|\mathcal{C}_7|^2 \\ &\quad + 12u_H(1-u_H)(u_H - s_H)\,{\rm Re}[\mathcal{C}_7\mathcal{C}_9^*] + (1-u_H)(u_H - s_H)(s_H - u_H^2)\,{\rm Re}[\mathcal{C}_{10a}\mathcal{C}_{10b}^*] \\ &\quad + \frac{(u_H - s_H)(s_H - u_H^2)^2}{4u_H}|\mathcal{C}_{10b}|^2\Big\}, \\ K^s(s_H, u_H) &= \frac{-12(s_H - u_H^2)^2(u_H - s_H)(1-u_H)}{u_H^4}\Big\{{\rm Re}[\mathcal{C}_9\mathcal{C}_{10a}^*] + \frac{2u_H}{u_H - s_H}{\rm Re}[\mathcal{C}_7\mathcal{C}_{10a}^*]\Big\}, \end{aligned} \tag{89}$$

and the limits with q^2 and m_X cuts are

$$\begin{gathered} 0 \le s_H \le s_H^0, \qquad \max\{s_H, u_1(s_H)\} \le u_H \le \min\{\sqrt{s_H}, u_2(s_H)\}, \\ u_1(s_H) = \frac{1 + s_H - y_H^{\min} - \sqrt{(1 + s_H - y_H^{\min})^2 - 4s_H}}{2}, \qquad u_2(s_H) = \frac{1 + s_H - y_H^{\max} - \sqrt{(1 + s_H - y_H^{\max})^2 - 4s_H}}{2}. \end{gathered} \tag{90}$$

D. $d^2\Gamma/dq^2 dp_X^+$ spectrum with q^2 and m_X cuts

From Eqs. (65) and the above results, we can obtain the dilepton invariant-mass spectrum and forward-backward asymmetry, for example, by integrating the doubly differential spectra

$$\begin{aligned} \frac{1}{\Gamma_0}\frac{d^2\Gamma}{dy_H du_H} &= H^y(y_H, u_H) m_B F^{(0)}\Big(m_B u_H, m_B \frac{1 - y_H - u_H}{1 - u_H}\Big), \\ \frac{1}{\Gamma_0}\frac{d^2 A_{\rm FB}}{dy_H du_H} &= K^y(y_H, u_H) m_B F^{(0)}\Big(m_B u_H, m_B \frac{1 - y_H - u_H}{1 - u_H}\Big) \end{aligned} \tag{91}$$

over u_H. Here

$$\begin{aligned} H^y(y_H, u_H) &= \frac{4[(1-u_H)^2 - y_H]^2}{y_H(1-u_H)^3}\Big\{y_H[(1-u_H)^2 + 2y_H](|\mathcal{C}_9|^2 + |\mathcal{C}_{10a}|^2) + [8(1-u_H)^2 + 4y_H]|\mathcal{C}_7|^2 \\ &\quad + 12y_H(1-u_H)\,{\rm Re}[\mathcal{C}_7\mathcal{C}_9^*] + y_H[(1-u_H)^2 - y_H]\,{\rm Re}[\mathcal{C}_{10a}\mathcal{C}_{10b}^*] + \frac{y_H[(1-u_H)^2 - y_H]^2}{4(1-u_H)^2}|\mathcal{C}_{10b}|^2\Big\}, \\ K^y(y_H, u_H) &= \frac{-12y_H[(1-u_H)^2 - y_H]^2}{(1-u_H)^3}\Big\{{\rm Re}[\mathcal{C}_9\mathcal{C}_{10a}^*] + \frac{2(1-u_H)}{y_H}{\rm Re}[\mathcal{C}_7\mathcal{C}_{10a}^*]\Big\}, \end{aligned} \tag{92}$$

and the limits of integration with cuts are

$$y_H^{\min} < y_H < y_H^{\max}, \qquad 0 \le u_H \le \min\Big\{1 - \sqrt{y_H}, \frac{1 + s_H^0 - y_H - \sqrt{(1 + s_H^0 - y_H)^2 - 4s_H^0}}{2}\Big\}. \tag{93}$$

The opposite order of integration is also useful:

$$0 \le u_H \le 1, \qquad y_1(u_H) < y_H < y_2(u_H),$$
$$y_1(u_H) = \max\left\{y_H^{\min}, \frac{(1-u_H)(u_H - s_H^0)}{u_H}\right\}, \qquad y_2(u_H) = \min\{y_H^{\max}, (1-u_H)^2\}. \tag{94}$$

The doubly differential rate can also be expressed in terms of the coefficients $C_9^{\rm mix}$, $C_7^{\rm mix}$, and C_{10}. This is one step closer to the short-distance coefficients C_9, C_7, and C_{10} of H_W, which we wish to measure in order to test the standard model predictions for the corresponding FCNC interactions. Substituting Eq. (33) into Eq. (92) gives

$$\begin{aligned} H^y(y_H, u_H) &= \frac{4[(1-u_H)^2 - y_H]^2}{(1-u_H)^3}\bigg\{|C_7^{\rm mix}(s,\mu_0)|^2\bigg[4\Omega_C^2(s,\mu_b) + \frac{8(1-u_H)^2}{y_H}\Omega_D^2(s,\mu_b)\bigg] \\ &\quad + [|C_9^{\rm mix}(s,\mu_0)|^2 + C_{10}^2][2y_H\Omega_A^2(s,\mu_b) + (1-u_H)^2\Omega_B^2(y_H,u_H,s,\mu_b)] \\ &\quad + {\rm Re}[C_7^{\rm mix}(s,\mu_0)C_9^{\rm mix}(s,\mu_0)^*][12(1-u_H)\Omega_E(s,\mu_b)]\bigg\} \\ K^y(y_H,u_H) &= \frac{-12y_H[(1-u_H)^2 - y_H]^2}{(1-u_H)^3}\bigg\{{\rm Re}[C_9^{\rm mix}(s,\mu_0)C_{10}^*]\Omega_A^2(s,\mu_b) + \frac{2(1-u_H)}{y_H}{\rm Re}[C_7^{\rm mix}(s,\mu_0)C_{10}^*] \\ &\quad \times \Omega_A(s,\mu_b)\Omega_D(s,\mu_b)\bigg\}, \end{aligned} \tag{95}$$

where $s = q^2/m_b^2$ and

$$\Omega_A = 1 + \frac{\alpha_s(\mu_b)}{\pi}\omega_a^V(s,\mu_b), \qquad \Omega_B = 1 + \frac{\alpha_s(\mu_b)}{\pi}\bigg[\omega_a^V(s,\mu_b) + \omega_c^V(s,\mu_b) + \frac{(1-u_H)^2 - y_H}{2(1-u_H)^2}\omega_b^V(s,\mu_b)\bigg],$$
$$\Omega_C = 1 + \frac{\alpha_s(\mu_b)}{\pi}[\omega_a^T(s,\mu_b) - \omega_b^T(s,\mu_b) - \omega_d^T(s,\mu_b)], \tag{96}$$
$$\Omega_D = 1 + \frac{\alpha_s(\mu_b)}{\pi}\bigg[\omega_a^T(s,\mu_b) - \omega_c^T(s,\mu_b) - \frac{(1-u_H)^2 + y_H}{2(1-u_H)^2}\omega_b^T(s,\mu_b)\bigg], \qquad \Omega_E = (2\Omega_A\Omega_D + \Omega_B\Omega_C)/3.$$

This is the form that turned out to be the most useful for the analysis in Ref. [30].

E. Numerical analysis of Wilson coefficients

As shown in Fig. 1, for the small-q^2 window ($q^2 < 6$ GeV^2) we have $p_X^+ \ll p_X^-$. Generically, the hard contributions in $\mathcal{C}_9$, $\mathcal{C}_7$, and $\mathcal{C}_{10a,10b}$ from our split-matching procedure depend on the variable q^2. In Fig. 5 we plot the q^2 dependence of the real part of the coefficients and see that there is in fact very little numerical change over the low-
q^2 window. Here Re$[C_9^{\rm local}]$ varies by $\pm1.5\%$, Re$[C_9^{\rm mix}]$ by $\pm1\%$, and the real parts of $\{\mathcal{C}_9, \mathcal{C}_7, \mathcal{C}_{10a}, \mathcal{C}_{10b}\}$ by $\{\pm1\%, \pm5\%, \pm2\%, \pm3\%\}$. The imaginary parts are either very small or also change by only a few percent over the low-q^2 window. The analytic formulas for the q^2 dependence mean that there is no problem keeping the exact dependence, but this does make it necessary to perform integrals over regions in q^2 numerically. A reasonable first approximation can actually be obtained by fixing a constant q^2 in the hard coefficients, while keeping the full q^2 dependence elsewhere.

Since the coefficients change very little with q^2 we continue our numerical analysis by fixing $q^2 = 3$ GeV^2. If we then take $\mu_0 = \mu_b = m_b = 4.8$ GeV, $\bar{m}_b(\mu_0) = 4.17$ GeV, $m_c/m_b = 0.292$ and $p_X^+ = 0$ we find that Eq. (33) gives

$$\begin{aligned} \mathcal{C}_9 &= 0.826C_9^{\rm mix} + 0.097C_7^{\rm mix} \\ &= 3.448\frac{C_9^{\rm mix}}{C_9^{\rm NDR}} - 0.030\frac{C_7^{\rm mix}}{C_7^{\rm NDR}}, \\ \mathcal{C}_7 &= 0.823C_7^{\rm mix} + 0.001C_9^{\rm mix} \\ &= -0.239\frac{C_7^{\rm mix}}{C_7^{\rm NDR}} + 0.005\frac{C_9^{\rm mix}}{C_9^{\rm NDR}}. \end{aligned} \tag{97}$$

These numbers indicate that, despite the entanglement of $C_{7,9}^{\rm mix}$ in $\mathcal{C}_{7,9}$ due to $\alpha_s(m_b)$ corrections, numerically $\mathcal{C}_9$ is dominated by C_9 and $\mathcal{C}_7$ is dominated by C_7 in the standard model.

For the coefficients at $q^2 = 3.0$ GeV^2, with the other parameters as above, we have

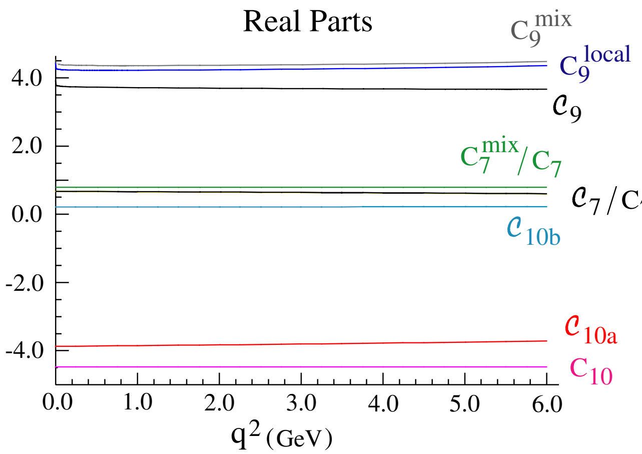

FIG. 5 (color online). Comparison of the real part of Wilson coefficients at $\mu_0 = \mu_b = 4.8$ GeV with $m_c/m_b = 0.292$, $\bar{m}_b(\mu_0) = 4.17$ GeV, and $m_b = 4.8$ GeV. For $\mathcal{C}_9$, $\mathcal{C}_7$, and $\mathcal{C}_{10b}$ we take $p_X^+ = 0$.

$$\begin{aligned} C_9^{\rm mix} &= 4.487 + 0.046i, \\ C_7^{\rm mix} &= -0.248, \\ \mathcal{C}_9(u_H = 0) &= 3.683 + 0.038i, \\ \mathcal{C}_7(u_H = 0) &= -0.198 + 6\times 10^{-5} i, \\ \mathcal{C}_9(u_H = 0.2) &= 3.663 + 0.038i \\ \mathcal{C}_7(u_H = 0.2) &= -0.193 + 10^{-4} i, \\ \mathcal{C}_{10a} &= -3.809, \\ \mathcal{C}_{10b}(u_H = 0) &= 0.214, \\ \mathcal{C}_{10b}(u_H = 0.2) &= 0.237. \end{aligned} \tag{98}$$

The relevant range of p_X^+ in Fig. 1 gives $0 \le u_H \le 0.2$. From the above numbers it is easy to see that the u_H dependence of $\mathcal{C}_9$, $\mathcal{C}_7$, and C_{10b} is very mild over the range of interest. The perturbative α_s corrections due to $\omega_i^{V,T}$ reduce both $\mathcal{C}_9$ and $\mathcal{C}_7$ by 17% relative to $C_9^{\rm mix}$ and $C_7^{\rm mix}$ respectively, and $\mathcal{C}_{10a}$ by 15%. This can be seen both in Fig. 5 and in Eq. (98), when one notes that $C_{10} = -4.480$. Comparing with coefficients in the local OPE, we note that the $\omega_{\rm semi}^{\rm OPE}$ factor, which accounts for the difference between $C_9^{\rm local}$ and $C_9^{\rm mix}$, is significantly smaller than the combination of α_s corrections in the ω_i^V terms that shifts $\mathcal{C}_9$ from its lowest-order value.

In quoting the above numbers, we have not varied the scales μ_0 and μ_b. The main point was to compare the size of the hard corrections in the shape-function and local OPE regions, and to see how much deviation from $C_{7,9}^{\rm mix}$ they cause. The dependence on μ_0 for the $\mathcal{C}_i$ is similar to that in the local OPE analysis at NLL [10,11] and will be reduced by a similar amount when the full NNLL expressions are included in $C_{7,9}^{\rm mix}$. The μ_b dependence of the $\mathcal{C}_i$ is fairly strong because of the appearance of double logarithms, but it is canceled by the μ_b dependence in the function $F^{(0)}$, which contains the NLL jet and shape functions.

IV. CONCLUSION

In this paper we have performed a model-independent analysis of $B \to X_s \ell^+ \ell^-$ decays with cuts giving the small-q^2 window and an m_X cut to remove $b \to c$ backgrounds. These cuts put us in the shape-function region. We analyzed the rate for the formal counting with $q^2 \sim \lambda^0$ and $m_X^2 \sim \lambda^2$ and showed that the same universal shape function as in $B \to X_u \ell \bar{\nu}$ and $B \to X_s \gamma$ is the only nonperturbative input needed for these decays. We also developed a new effective-theory technique of split matching. Split matching between two effective theories is done not at a single scale μ, but rather at two nearby scales. For $B \to X_s \ell^+ \ell^-$ this allowed us to decouple the perturbation-theory analysis above and below m_b, which simplifies the organization of the α_s contributions.

In Sec. III we presented the leading-power triply differential spectrum and doubly differential forward-backward asymmetry with renormalization-group evolution and matching to $\mathcal{O}(\alpha_s)$. Above the scale m_b, we restricted our analysis to include the standard NLL terms from the local OPE, but illustrated how terms from NNLL can be incorporated. Below m_b we considered running to NLL and matching at one-loop (NNLL evolution will be straightforward to incorporate if desired). We then computed several phenomenologically relevant doubly differential spectra with phase-space cuts on q^2 and m_X (from which the singly differential spectra can be obtained by numerical integration). In Sec. III E we discussed the numerical size of our perturbative hard coefficients and compared them to the local OPE results.

Our results for the doubly differential rate in Eqs. (91) and (92), together with $F^{(0)}$ from Eq. (81), determine the shape-function-dependent rate for $B \to X_s \ell^+ \ell^-$. Using as input a result for the nonperturbative shape function $f^{(0)}$ from a fit to the $B \to X_s \gamma$ spectrum or from $B \to X_u \ell \bar{\nu}$ gives a model-independent result for $B \to X_s \ell^+ \ell^-$ with phase-space cuts. A full investigation of the m_X-cut dependence and phenomenology is carried out in a companion publication [30]. An intriguing universality of the cut dependence is found, which makes the experimental extraction of short-distance Wilson coefficients in the presence of cuts much simpler. An extension of the analysis of this paper to include subleading shape-function effects will be presented in the near future [57].

ACKNOWLEDGMENTS

We thank Z. Ligeti and F. Tackmann for helpful discussions and for collaboration on a related analysis of $B \to X_s \ell \ell$, and D. Pirjol for comments on the manuscript. This work was supported in part by the U.S. Department of Energy (DOE) under the cooperative research agreement

No. DF-FC02-94ER40818 and by the Office of Nuclear Science. I. S. was also supported in part by the DOE Outstanding Junior Investigator program and the Sloan Foundation.

APPENDIX A: WILSON COEFFICIENTS

The coefficients and functions that appear in Eq. (6) are defined as follows [10].

$$C_7(M_W) = -\frac{1}{2}A(m_t^2/M_W^2), \qquad C_8(M_W) = -\frac{1}{2}F(m_t^2/M_W^2), \qquad Y(x) = C(x) - B(x), \qquad Z(x) = C(x) + \frac{1}{4}D(x),$$

$$A(x) = \frac{x(8x^2+5x-7)}{12(x-1)^3} + \frac{x^2(2-3x)}{2(x-1)^4}\ln x, \qquad B(x) = \frac{x}{4(1-x)} + \frac{x}{4(x-1)^2}\ln x,$$

$$C(x) = \frac{x(x-6)}{8(x-1)} + \frac{x(3x+2)}{8(x-1)^2}\ln x, \qquad D(x) = \frac{-19x^3+25x^2}{36(x-1)^3} + \frac{x^2(5x^2-2x-6)}{18(x-1)^4}\ln x - \frac{4}{9}\ln x,$$

$$E(x) = \frac{x(18-11x-x^2)}{12(1-x)^3} + \frac{x^2(15-16x+4x^2)}{6(1-x)^4}\ln x - \frac{2}{3}\ln x, \qquad F(x) = \frac{x(x^2-5x-2)}{4(x-1)^3} + \frac{3x^2}{2(x-1)^4}\ln x,$$

and

$$t_i = \left(2.2996, -1.0880, -\frac{3}{7}, -\frac{1}{14}, -0.6494, -0.0380, -0.0186, -0.0057\right),$$

$$a_i = \left(\frac{14}{23}, \frac{16}{23}, \frac{6}{23}, -\frac{12}{23}, 0.4086, -0.4230, -0.8994, 0.1456\right),$$

$$p_i = \left(0, 0, -\frac{80}{203}, \frac{8}{33}, 0.0433, 0.1384, 0.1648, -0.0073\right),$$

$$\rho_i^{\rm NDR} = (0, 0, 0.8966, -0.1960, -0.2011, 0.1328, -0.0292, -0.1858),$$

$$s_i = (0, 0, -0.2009, -0.3579, 0.0490, -0.3616, -0.3554, 0.0072),$$

$$q_i = (0, 0, 0, 0, 0.0318, 0.0918, -0.2700, 0.0059).$$

APPENDIX B: THE CASE OF COLLINEAR q^2

In the body of the paper we used $q^2 \sim \lambda^0$. We were free to choose this counting since the power counting for the leptonic variable q^2 does not affect the counting for $p_X^\pm$ in the shape-function region. (The only restriction was not to have q^2 too close to m_b^2.) However, we are free to consider other choices. In this appendix we consider how our analysis will change if we instead take $q^2 \sim \lambda^2$. With this scaling, new physical degrees of freedom are needed at leading order in SCET, making the analysis more complicated. In particular we must consider graphs with quark fields that are collinear to the collinear photon (or dilepton pair), since with this power counting we have $(q^0)^2 \gg q^2$.

An example of a new *nonzero* graph is the one generated by four-quark operators within SCET, as shown in Fig. 6, which involve these additional degrees of freedom. In this graph we have a light-quark loop of collinear-$\bar{n}$ fields that are collinear to the virtual photon. The presence of this type of diagram changes the hard matching at $\mu_b = m_b$. It also means that we have a more complicated pattern of operator mixing within SCET, since divergences in the displayed diagram will cause an evolution for C_9, etc. Therefore, the running below m_b will no longer be universal. In the presence of these diagrams the jet function will also no longer be given by a single bilinear operator, since it will also involve some contributions with a factorized matrix element of $\bar{n}$-fields, which are also integrated out at $p^2 \sim m_b\Lambda_{\rm QCD}$. Finally, the appearance of these additional degrees of freedom might also affect the number of nonperturbative shape functions that appear in the factorization theorem. It would be interesting to carry out a detailed analysis of this $q^2 \sim \lambda^2$ case in the future.

In $B \to X_s\gamma$ at lowest order, the analog of the graph in Fig. 6 vanishes at one-loop order, and this argument can be extended to include higher orders in α_s [44]. This relies on the fact that here $q^2 = 0$ and does not generate a scale. We find that the same reasoning does not apply for $B \to X_s\ell\ell$ for parametrically small but finite q^2.

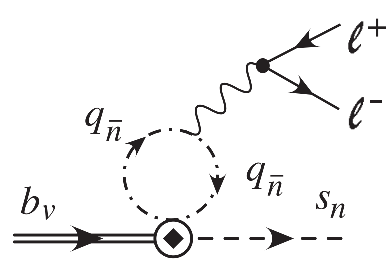

FIG. 6. Additional graphs in SCET for the matching computation for the case where $q^2 \sim \lambda^2$.

Finally, we comment on the possibility of penguin charm-loop effects. In our analysis we integrated out the charm loops at the same time as the bottom loops. This is reasonable when treating $q^2 \sim \lambda^0$. One could also consider the case $m_c^2 \sim m_b \Lambda$, which is also reasonable numerically. This type of power counting was considered for the simpler case of $B \to X_c \ell \bar{\nu}$ decays with energetic X_c in Ref. [58] and it would be interesting to extend this to $B \to X_s \ell\ell$. We remark that the problematic region for $B \to \pi\pi$ factorization theorems [59–62], which is near the charm threshold, $q^2 \sim 4m_c^2$, is not relevant for our analysis. The experimental cuts on q^2 explicitly remove the known large contributions from this region.

[1] M. S. Alam *et al.* (CLEO Collaboration), Phys. Rev. Lett. **74**, 2885 (1995).
[2] R. Barate *et al.* (ALEPH Collaboration), Phys. Lett. B **429**, 169 (1998).
[3] K. Abe *et al.* (Belle Collaboration), Phys. Lett. B **511**, 151 (2001).
[4] S. Chen *et al.* (CLEO Collaboration), Phys. Rev. Lett. **87**, 251807 (2001).
[5] B. Aubert *et al.* (*BABAR* Collaboration), hep-ex/0207074.
[6] J. Kaneko *et al.* (Belle Collaboration), Phys. Rev. Lett. **90**, 021801 (2003).
[7] B. Aubert *et al.* (*BABAR* Collaboration), hep-ex/0308016; Phys. Rev. Lett. **93**, 081802 (2004).
[8] M. Iwasaki *et al.* (Belle Collaboration), hep-ex/0503044.
[9] B. Grinstein, M. Savage, and M. B. Wise, Nucl. Phys. **B319**, 271 (1989).
[10] A. J. Buras and M. Münz, Phys. Rev. D **52**, 186 (1995).
[11] M. Misiak, Nucl. Phys. **B393**, 23 (1993); **B439**, 461(E) (1995).
[12] C. Bobeth, M. Misiak, and J. Urban, Nucl. Phys. **B574**, 291 (2000); K. G. Chetyrkin, M. Misiak, and M. Munz, Phys. Lett. B **400**, 206 (1997); **425**, 414(E) (1998).
[13] H. H. Asatryan, H. M. Asatrian, C. Greub, and M. Walker, Phys. Rev. D **65**, 074004 (2002); H. M. Asatrian, H. H. Asatryan, A. Hovhannisyan, and V. Poghosyan, Mod. Phys. Lett. A **19**, 603 (2004).
[14] A. Ghinculov, T. Hurth, G. Isidori, and Y.-P. Yao, Nucl. Phys. **B648**, 254 (2003); H. M. Asatrian, K. Bieri, C. Greub, and A. Hovhannisyan, Phys. Rev. D **66**, 094013 (2002).
[15] C. Bobeth, P. Gambino, M. Gorbahn, and U. Haisch, J. High Energy Phys. 04 (2004) 071.
[16] A. Ghinculov, T. Hurth, G. Isidori, and Y.-P. Yao, Nucl. Phys. **B685**, 351 (2004); Nucl. Phys. B, Proc. Suppl. **116**, 284 (2003).
[17] M. A. Shifman and M. B. Voloshin, Sov. J. Nucl. Phys. **41**, 120 (1985); J. Chay, H. Georgi, and B. Grinstein, Phys. Lett. B **247**, 399 (1990); I. I. Y. Bigi, N. G. Uraltsev, and A. I. Vainshtein, Phys. Lett. B **293**, 430 (1992); **297**, 477(E) (1993); A. V. Manohar and M. B. Wise, Phys. Rev. D **49**, 1310 (1994).
[18] A. V. Manohar and M. B. Wise, Cambridge Monogr. Part. Phys., Nucl. Phys., Cosmol. **10**, 1 (2000).
[19] A. F. Falk, M. E. Luke, and M. J. Savage, Phys. Rev. D **49**, 3367 (1994).
[20] A. Ali, G. Hiller, L. T. Handoko, and T. Morozumi, Phys. Rev. D **55**, 4105 (1997).
[21] C. W. Bauer and C. N. Burrell, Phys. Rev. D **62**, 114028 (2000); Phys. Lett. B **469**, 248 (1999).
[22] F. Krüger and L. M. Sehgal, Phys. Lett. B **380**, 199 (1996).
[23] J. W. Chen, G. Rupak, and M. J. Savage, Phys. Lett. B **410**, 285 (1997); G. Buchalla, G. Isidori, and S.-J. Rey, Nucl. Phys. **B511**, 594 (1998).
[24] M. Neubert, Phys. Rev. D **49**, 3392 (1994); **49**, 4623 (1994); I. I. Y. Bigi *et al.*, Int. J. Mod. Phys. A **9**, 2467 (1994).
[25] A. Ali and G. Hiller, Phys. Rev. D **58**, 074001 (1998); **60**, 034017 (1999).
[26] C. W. Bauer, S. Fleming, and M. E. Luke, Phys. Rev. D **63**, 014006 (2001).
[27] C. W. Bauer, S. Fleming, D. Pirjol, and I. W. Stewart, Phys. Rev. D **63**, 114020 (2001).
[28] C. W. Bauer and I. W. Stewart, Phys. Lett. B **516**, 134 (2001).
[29] C. W. Bauer, D. Pirjol, and I. W. Stewart, Phys. Rev. D **65**, 054022 (2002).
[30] K. S. M. Lee, Z. Ligeti, I. W. Stewart, and F. J. Tackmann, hep-ph/0512191.
[31] G. P. Korchemsky and G. Sterman, Phys. Lett. B **340**, 96 (1994).
[32] T. Mannel and S. Recksiegel, Phys. Rev. D **63**, 094011 (2001).
[33] C. W. Bauer and A. V. Manohar, Phys. Rev. D **70**, 034024 (2004).
[34] S. W. Bosch, B. O. Lange, M. Neubert, and G. Paz, Nucl. Phys. **B699**, 335 (2004).
[35] C. W. Bauer, M. E. Luke, and T. Mannel, Phys. Rev. D **68**, 094001 (2003).
[36] A. K. Leibovich, Z. Ligeti, and M. B. Wise, Phys. Lett. B **539**, 242 (2002).
[37] C. W. Bauer, M. E. Luke, and T. Mannel, Phys. Lett. B **543**, 261 (2002).
[38] K. S. M. Lee and I. W. Stewart, Nucl. Phys. **B721**, 325 (2005).
[39] S. W. Bosch, M. Neubert, and G. Paz, J. High Energy Phys. 11 (2004) 073.
[40] M. Beneke, F. Campanario, T. Mannel, and B. D. Pecjak, J. High Energy Phys. 06 (2005) 071.
[41] B. O. Lange, J. High Energy Phys. 01 (2006) 104.
[42] A. K. Leibovich and I. Z. Rothstein, Phys. Rev. D **61**, 074006 (2000).
[43] A. K. Leibovich, I. Low, and I. Z. Rothstein, Phys. Rev. D **62**, 014010 (2000).
[44] M. Neubert, Eur. Phys. J. C **40**, 165 (2005).
[45] A. K. Leibovich, I. Low, and I. Z. Rothstein, Phys. Rev. D

62, 014010 (2000); **61**, 053006 (2000).
[46] J. Chay, C. Kim, and A. K. Leibovich, Phys. Rev. D **72**, 014010 (2005).
[47] B. Grinstein and D. Pirjol, hep-ph/0505155.
[48] C. Greub, T. Hurth, and D. Wyler, Phys. Rev. D **54**, 3350 (1996).
[49] A. J. Buras, A. Czarnecki, M. Misiak, and J. Urban, Nucl. Phys. **B631**, 219 (2002).
[50] G. P. Korchemsky and A. V. Radyushkin, Nucl. Phys. **B283**, 342 (1987); I. A. Korchemskaya and G. P. Korchemsky, Phys. Lett. B **287**, 169 (1992).
[51] S. Moch, J. A. M. Vermaseren, and A. Vogt, Nucl. Phys. **B688**, 101 (2004).
[52] B. O. Lange, M. Neubert, and G. Paz, J. High Energy Phys. 10 (2005) 084.
[53] B. O. Lange, M. Neubert, and G. Paz, Phys. Rev. D **72**, 073006 (2005).
[54] F. J. Tackmann, Phys. Rev. D **72**, 034036 (2005).
[55] C. Balzereit, T. Mannel, and W. Kilian, Phys. Rev. D **58**, 114029 (1998).
[56] C. N. Burrell, M. E. Luke, and A. R. Williamson, Phys. Rev. D **69**, 074015 (2004).
[57] K. S. M. Lee *et al.* (unpublished).
[58] H. Boos, T. Feldmann, T. Mannel, and B. D. Pecjak, Phys. Rev. D **73**, 036003 (2006).
[59] C. W. Bauer, D. Pirjol, I. Z. Rothstein, and I. W. Stewart, Phys. Rev. D **70**, 054015 (2004).
[60] T. Feldmann and T. Hurth, J. High Energy Phys. 11 (2004) 037.
[61] M. Beneke, G. Buchalla, M. Neubert, and C. T. Sachrajda, Phys. Rev. D **72**, 098501 (2005).
[62] C. W. Bauer, D. Pirjol, I. Z. Rothstein, and I. W. Stewart, Phys. Rev. D **72**, 098502 (2005).